Studies of Plume Condensation Contamination upon Surfaces of the Terrestrial Planet Finder Spacecraft

By

Timothy David Pigeon
B.S., Massachusetts Institute of Technology, Cambridge, MA, 2003

Submitted to the Department of Aeronautics and Astronautics
in partial fulfillment of the requirements for the degree of

Master of Science in Aeronautics and Astronautics

at the

MASSACHUSETTS INSTITUTE OF TECHNOLOGY

September 2005

Author…….....
Department of Aeronautics and Astronautics
August 3rd, 2005

Certified by……..
Manuel Martínez-Sánchez
Professor of Aeronautics and Astronautics
Thesis Supervisor

Accepted by…….
Jaime Peraire
Professor of Aeronautics and Astronautics
Chair, Committee on Graduate Students

Acknowledgments

Prof. Manuel Martinez-Sanchez – Thanks for all of the insights into the various phenomena at play in this project, and for being so knowledgeable about so many areas both directly and indirectly related to space propulsion issues. In addition, your classes that I took were quite helpful in building a base of propulsion knowledge.

Dr. Paulo Lozano – Thanks for all of the help setting up my experiment, as well as diagnosing the various issues that came up, not just limited to piping concerns and repairing tank leaks.

Prof. Smith, Mike, and Don from the MIT Cryogenics Lab – Thanks for enlightening me about the wonderful world of liquid helium research, for answering my many questions about it, and also for supplying so much helium so promptly.

SPL Labmates – Thanks for the support, and Murat in particular for tackling the TPF project with me.

The JPL Team – Thanks for answering my questions and concerns promptly, even when the questions could not yet be answered.

Ryan, Kris, Mom, and others – Thanks for keeping me grounded all this time, and for listening to my lamentations.

Abstract

There are two competing concepts for the Terrestrial Planet Finder (TPF) mission, one which involves a single spacecraft, and another comprised of a five craft formation. In addition, there are several propulsion options under consideration. Unique contamination issues affect the formation-flying concept due to the close proximity of the spacecrafts. Select surfaces must be maintained at the low temperature of 40 K. There is concern that propellant expelled from one craft will condense on the cryogenic surfaces of a neighboring craft, adversely affecting performance and the integrity of the observational data. The condensation properties of warm Xenon, Krypton, and Argon upon a cryogenically-chilled QCM were characterized at a range of temperatures and pressures. Heats of adsorption were predicted with a model to solve for intermolecular forces, and experimental data was used to assess the model's validity. Knowledge of the heat of adsorption was used to determine the equilibrium level of surface coverage for both a pulsed and constant operation thruster, for a range of impinging gas fluxes. The model aims to aid in the selection of an appropriate propulsion system and propellant for the TPF spacecraft.

Table of Contents

I. Introduction 6
A. The TPF Project 6
B. TPF Propulsion Options 8
C. Project Objectives 9
D. TPF Mission Profile 10
E. Previous Work 10
II. Model 14
A. Introduction 14
B. The Model 14
1. Sticking Coefficient 16
2. Flux 18
3. Residence Time 19
a. Derivation of the Heat of Adsorption 19
b. Heat of Adsorption Non-Idealities 23
c. Applying the Heat of Adsorption to the Model 27
4. Density of a Monolayer 30
III. Model Predictions 32
A. Spreadsheet Setup 32
B. TPF-specific Modeling 34
1. Direct vs. Indirect Flux 35
2. Pulsed Thrusters 36
3. Continuous Thrusters 39
4. Expected Thruster Flux 41
IV. Experimental Setup 46
A. Motivation 46
B. Equipment 47
C. QCM Theory 47
D. Cooling Circuit 49
V. Testing 53
VI. Testing Results and Analysis 56
A. Testing Conditions 56
B. Data Reduction Process 57
C. Errors 59
D. Results 60
1. Xenon 60
2. Krypton 62
E. Interpretations 64
VII. Recommendations 65
VIII. Conclusion 69
Appendix A – Data Plots 71
Appendix B – Instructions 75
A. Using Liquid Helium 75
B. Using Liquid Nitrogen 78
C. Flowing the Test Gas 79
D. Operating the QCM Software 80
Citations 81

Table of Figures

Figure 1. TPF cluster, combiner (top), and four collectors. 7
Figure 2. TPF collector craft dark side, observing (left); sun side (right) 8
Figure 3. Saturation pressure plots using the Clausius-Clapeyron equation. 13
Figure 4. Example dispersion potential, r_0 = 3 Å 21
Figure 5. Ideal heat of adsorption with perfect surface, no adsorbate interactions. 24
Figure 6. Surface irregularities, no adsorbate interactions. 24
Figure 7. Heat of adsorption with adsorbate interactions. 25
Figure 8. Realistic heat of adsorption vs. coverage behavior. 27
Figure 9. Cubic structure and allowed positions of gas atoms. 28
Figure 10. Modeled heat of adsorption, surface flaws and adatom interactions. 30
Figure 11. Sample plot of steady Argon flux, then turned off. 33
Figure 12. Model deposition profile with tank base pressure of 10^{-8} Torr. 34
Figure 13. Direct vs. indirect flux 36
Figure 14. Equilibrium deposition behavior with pulsed thrusters 38
Figure 15. Equilibrium coverage for various heats of adsorption vs. pulsed flux ... 38
Figure 16. Sample deposition vs. time for continuous thrusting, constant flux 40
Figure 17. Equilibrium coverage for various heats of ads. vs. continuous flux 41
Figure 18. Ion and neutral downstream spreading 43
Figure 19. BHT-200 ion current density. 43
Figure 20. Neutral flow into vacuum from an orifice. 44
Figure 21. Experimental setup schematic. 46
Figure 22. MK16 CQCM model. 49
Figure 23. Feedthrough/coil (top), adapter (left), QCM connector (right). 50
Figure 24. Inside the vacuum chamber. 51
Figure 25. Overall view. 52
Figure 26. Xenon plot showing raw data and treated data. 58
Figure 27. Xenon heat of adsorption vs. coverage, by temperature 61
Figure 28. Xenon heat of adsorption data with trendline 61
Figure 29. Krypton heat of adsorption vs. coverage, by temperature 62
Figure 30. Krypton heat of adsorption data with trendline 63
Figure 31. Expected equilibrium coverages for real and modeled data. 66
Figure A1-A5. Xenon plots at each temperature 73
Figure A6-A8. Krypton plots at each temperature 74
Figure B1. Liquid helium dewar ports 76

I. Introduction

A. The TPF Project

The Terrestrial Planet Finder (TPF) represents a telescope project that is a part of NASA's Origins program.[1] The objective of the TPF project is to search for planets in neighboring star systems that have the molecular components that are elemental to all known forms of life. This mission requires novel imaging techniques due to the extreme resolution demanded to detect Earth-like bodies light years distant. The extrasolar planets that have been discovered thus far are typically large gas giants orbiting close to their parent star. The combination of size and proximity results in a mutual gravitational pull that induces a measurable wobble in the star's location as the planet orbits about the star.

The TPF telescopes will tackle the detection problem in a more direct manner, by attempting to locate specific bio-markers given off by a suspect planet. These markers are radiation of known frequencies in the infrared and near-IR range, characteristic of various modes of compounds such as diatomic oxygen, carbon dioxide, methane, ozone, and water. Detection is made vastly more difficult by the presence of the planet's home star. The star's intensity is on the order of a billion times greater than that of the target planet, so negating the star's light while viewing the planet is critical. The TPF team has created two competing architectures under consideration. One concept is a single spacecraft housing a large coronagraph that will measure in the visible and near-infrared region of the electromagnetic spectrum. The second concept is to use a nulling infrared interferometer to block out the starlight. This must be accomplished with a number of interferometry instruments, set tens of meters apart, which leaves only two options: a large, connected truss structure, or multiple formation-flying spacecrafts. The TPF team has chosen to develop a formation flying approach consisting of four collector spacecraft and one combiner, as shown in Figure 1.

Figure 1. TPF cluster, combiner (top), and four collectors.

A formation flying approach carries a set of unique problems not encountered on single-craft missions, particularly in the areas of orientation and spacecraft interaction issues. In the TPF interferometry architecture, the spacecraft are in close enough proximity where the plumes of the thrusters of a neighboring spacecraft can have tangible effects. There are issues of radiation contamination caused by the energized plume particles where they may give off photons in the observational frequency range. In addition there is the issue of physical contamination caused by deposition and condensation of propellant particles upon critical surfaces of a neighboring satellite, mostly the gold-plated mirrors. Complicating this problem is the fact that the interferometry instruments, though protected from its own thrusters by a sun shield, must be cryogenically cooled to 40 K. This low temperature raises the concern of the propellant gas freezing on the surface creating a liquid layer that grows over time, corrupting the observations.

The current spacecraft design involves a large, four-sided sun shield protecting the interferometers from the Sun's light. The necessary spacecraft infrastructure will be positioned on the warm side, as shown in Figure 2. Orientation control will be controlled

for clusters of four thrusters on each of the four corners of the sun shield, directed away from the interferometry instruments.

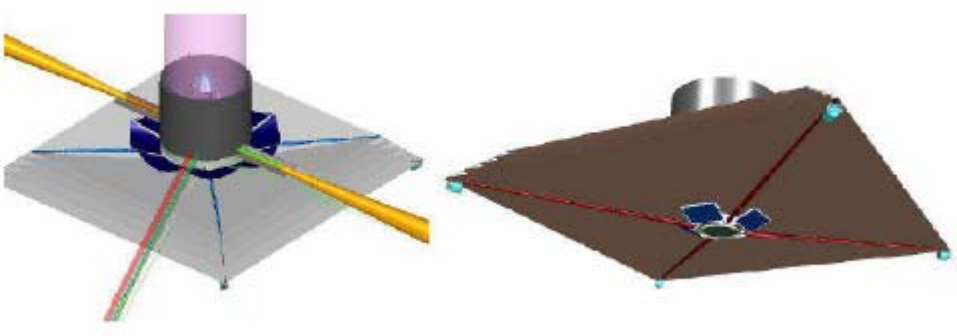

Figure 2. TPF collector craft dark side, observing (left); sun side (right)

B. TPF Propulsion Options

The size of the spacecraft and the maneuvers required demand a propulsion system with thrust in the 0.1-25mN range. There are several viable options available that can provide precise performance in that thrust range, most of which involve inert propellants. The simplest system would use cold gas thrusters. In this case, a gas, such as nitrogen, is stored at high pressure in a tank, and released in small amounts through a valve. The flow is expanded to higher speed through a nozzle. This process results in a low specific impulse (Isp) of around 70 sec. Isp is a measure of propulsion system efficiency, and is directly proportional to the gas exit velocity. With higher Isp values, the same total impulse can be delivered with a lower propellant mass, saving valuable weight.

Higher Isp options involve electric propulsion (EP) schemes. In EP systems, electrical power is used to add energy to the gas flow, and this power is generated by an onboard power processing unit. The vast majority of spacecraft draw their power from photovoltaic solar panels. A resistojet is the simplest form of EP, as it uses electrical power to heat a channel through which gas flows through. The gas molecules collide with the heated walls and gain energy, and thus, velocity.

More complicated systems under consideration involve pulsed plasma thrusters and electromagnetic schemes. A pulsed plasma thruster operates by unleashing a high-voltage discharge across the face of a Teflon stick. A small amount of the Teflon is ionized during each pulse, and accelerated out of the thruster. This system has the advantages of precise impulse on each pulse, as well as the ability to fire many times per second. Isp values are in the 600-1200 sec range. A Hall thruster is a mature technology, but requires a more complicated infrastructure. Halls operate by using electrons shed from an external cathode to ionize Xenon atoms, which are then accelerated away from an anode charged with a few hundred volts. A magnetic circuit is employed to trap electrons in an area known as the ionization region. Additional electrons from the cathode are sprayed downstream to neutralize the plume and the craft. Isp values are typically in the 1000-2000 sec. range, so that much less propellant is needed, although more electrical power is required. Hall thrusters are not as well suited for pulsed operations as other forms of propulsion.

C. Project Objectives

At the present time, the TPF propulsion systems have not been determined. Condensation is a phenomenon related primarily to the temperature of the gas and the surface, as well as the surface coverage and gas pressure, or density, at the surface in question. Since the propulsion systems are unknown, the propellant is unknown. In addition, critical parameters such as the mass flow, plume divergence angle, and exact orientation maneuvers are not available, which affects the particle flux reaching these critical surfaces.

To deal with the uncertainty of the propulsion systems, a general model has been developed based upon experimental data collection. The model provides a prediction of the mass deposition rate, and consequently, the growth rate in monolayers that can be expected based upon a few input parameters: propellant type, surface temperature, and gas partial pressure or flux at the surface.

Experiments have been conducted in a vacuum chamber that utilizes a cryogenically-cooled quartz crystal microbalance (QCM) to simulate a cooled satellite surface. The QCM inside the chamber is exposed to different gases at a range of different pressures, crystal temperatures, and gas temperatures. These tests are used to generate heat of adsorption values for the gases of interest, and to verify the model's accuracy. The ultimate goal of the project is to determine whether or not condensation will be an issue of concern for selected propulsion designs for the TPF project, and if so, to what extent.

D. TPF Mission Profile

The current profile for TPF is for the spacecraft constellation to fly in an Earth-trailing orbit – following the Earth in her orbital path, while not orbiting the Earth. This is of importance to the condensation issue because the constellation will be well beyond the Earth's exosphere. This exposes the TPF spacecraft to the hard vacuum of interplanetary space. Since condensation is directly related to pressure (flux), modeling is made simpler, as the only particle flux the units will encounter will come from the thrusters or negligible outgassing.

E. Previous Work

Surprisingly, the amount of relevant published data regarding spacecraft condensation is very limited. This is probably due to the fact that a small fraction of existing satellites are cryogenically cooled to such a low temperature range. Furthermore, there have not been any full-scale formation-flying spacecraft missions sent into orbit, so when spacecraft contamination is mentioned, it typically refers to outgassed particles and not propellant plumes. What further hampers the literature search is the fact that other published reports speak of internal models or Monte Carlo simulations.[2]

A paper by Scialdone [3] tackles the tangential problem of self-contamination via outgassing particles adsorbing and condensing. He describes the contamination problem as a two-regime problem. Initially, when the surface is bare, physical adsorption is

dominant, and it is an issue of physical and electrostatic forces. A fraction of colliding particles stick to the surface as a function of the sticking coefficient between the gas and the surface, and there is an average residence time for a particle to remain on the surface. If the impinging and departing fluxes reach an equilibrium state, the number of adsorbed particles per unit area, σ, is given by

$$\sigma = \alpha\phi\tau \tag{1}$$

where α is the sticking coefficient, ϕ is the impinging flux, and τ is the average residence time. Scialdone finds that the residence time is a function of surface lattice properties, the surface temperature, and the heat of adsorption of the gas,

$$\tau = \tau_o e^{Q/RT_s} \tag{2}$$

The period of oscillation of the adsorbed molecule perpendicular to the surface, τ_o, is assumed between 10^{-12} and 10^{-14} seconds, usually set at 1.0×10^{-13} seconds, Q is the heat of adsorption, and R is the gas constant.[2] As the deposition increases, the surface becomes more obscured, until fully covered by a thin layer of the substance, in liquid or solid form, a few monolayers thick. As the deposition proceeds from partial surface coverage to total surface coverage, the situation becomes one of a gas colliding with a surface of similar liquid.

In Scialdone's second regime, the gas partial pressure is greater than the saturation vapor pressure (SVP) of the gas at the surface temperature. When this occurs, general condensation begins, once the surface has attained a thin layer of 5-10 monolayers. Condensation is governed by the SVP, which is determined by the Clausius-Clapeyron equation:

$$P_{SVP} = P_{STD} * e^{\frac{\Delta H_{vap}}{RT}(\frac{T_s}{T_{BP}}-1)} \quad (3)$$

where P_{STD} is standard atmospheric pressure (1 atm), ΔH_{vap} is the heat of vaporization, T_{BP} is the boiling point of the gas at 1 atm, and T_s is the temperature of the condensing surface. A plot of the Clausius-Clapeyron equation for a number of gases is shown in Figure 3. This is used to find the SVP of a gas at a given surface temperature, where any pressure above the SVP will result in condensation. When the partial pressure exceeds the saturated vapor pressure, then the condensation rate is the difference between the impinging flux and the evaporation flux, which is governed by the saturation pressure.

$$\dot{\sigma}_c = \alpha_c(\phi - \phi_e) = \alpha_c\phi[1-(P_{SVP}/P_g)(T_g/T_s)^{1/2}] \quad (4)$$

Here, α_c is the condensation coefficient, ϕ_ε is the evaporation flux, and P_g and T_g are the pressure and temperature of the gas. When the gas pressure is at least a decade greater than the saturation pressure, the condensation coefficient can be assumed to be one. This regime is not of great consequence to the TPF mission. Any buildup beyond a few monolayers is probably unacceptable, as it will affect the optical, radiative, and electrical properties of the mirrors, so the surfaces should never be allowed into the liquid condensation regime. Furthermore, any temporary flux greater than the SVP will soon end, and the surrounding pressure will drop back down to the hard vacuum of space. This pressure drop will accelerate the evaporation of the accumulated liquid layer until only the few monolayers that are bound to the surface lattice remain.

Thus, the issue of greater concern is those first few monolayers. Assuming that the plume density, and exit velocity (hence, temperature) of the propellant is known, the impinging flux can be calculated. The adsorption rate becomes an issue of knowing the sticking coefficient and the resident time for a molecule to stay on the surface.

Difficulties concerning the determination of these two parameters will be discussed in depth in the Model chapter.

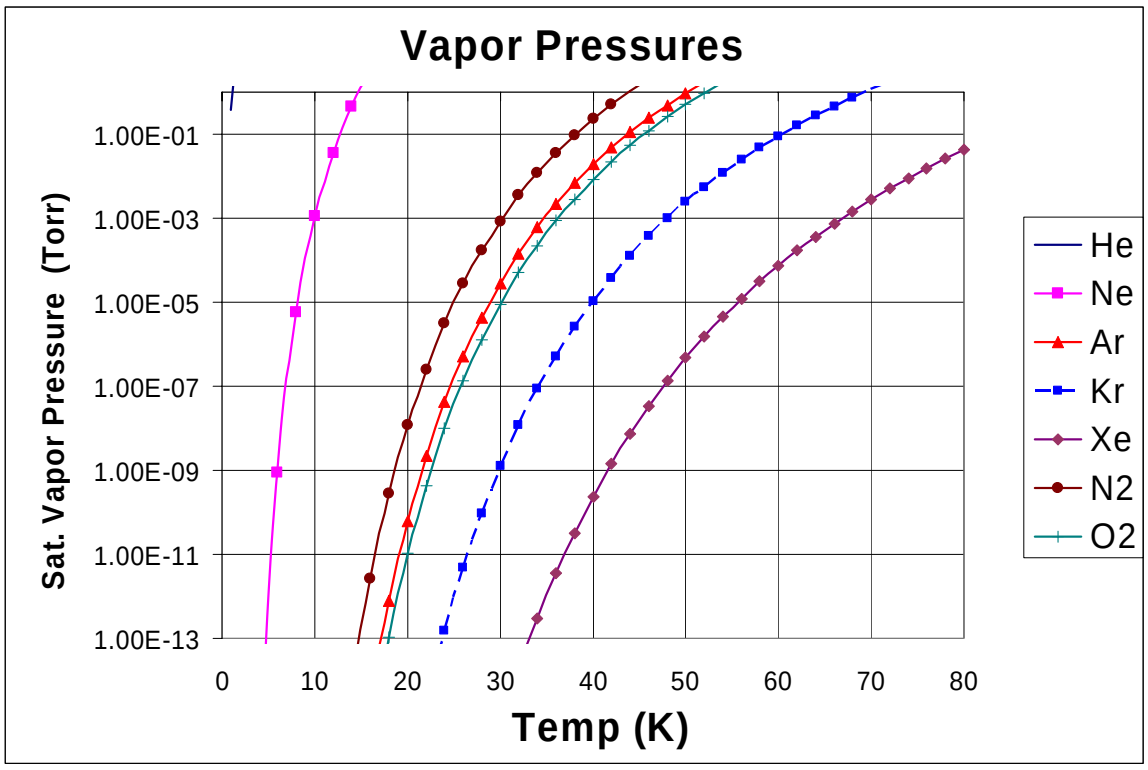

Figure 3. Saturation pressure plots using the Clausius-Clapeyron equation.

II. Model

A. Introduction

The goal of this research is to create a model that will determine whether or not the propellant expelled from orientation thrusters will condense on cryogenically-chilled surfaces of a neighboring spacecraft. At this stage, the TPF team is considering the use of electric propulsion (EP) systems, so the model will be tested against experimental results using typical EP propellants, such as Krypton and Xenon gas. There is also consideration of simpler, but less efficient, cold-gas or chemical thrusters that use nitrogen or hydrogen. The model is broad enough to where it should be valid for the evaluation of other mono- and bi-propellant chemical thrusters, but there will not be empirical results to confirm the model's validity for those substances.

B. The Model

Scialdone's first regime, where the partial gas pressure by the plate is less than the saturation vapor pressure, is deemed the more important of the two. This regime covers the first few monolayers of accumulated deposit, which is enough to cause problems with the interferometric equipment. Any additional condensation will quickly evaporate away once the thruster flow is cut anyway, back down to the level of a few monolayers, where gas-surface interactions dominate over gas-condensed liquid interaction.

At the heart of the model is a deposition rate equation from Chang's paper that accounts for the impinging flux that sticks to the surface, as well as the rate of desorption flux from the mass of molecules that have already stuck.[4] The equation is as follows:

$$\dot{\sigma} = \alpha\phi - \sigma/\tau \tag{5}$$

The first part of the equation is the depositing flux, where the sticking coefficient, α, is simply the fraction of the impinging flux, ϕ, that sticks to the surface. The negative contributor is the desorbing flux, which is the current deposition, σ (in molecules/area), divided by a residence time. With a constant incoming flux, it is plain to see that the deposition level will increase, until equilibrium is reached when the adsorbing and desorbing fluxes are equal. If α, ϕ, and τ are constant, then solving the differential equation, with an initial condition that there is no deposition at time = 0, yields the following equation for deposition:

$$\sigma(t) = \alpha\phi\tau(1 - e^{-t/\tau}) \tag{6}$$

But, the residence time varies with coverage, $\tau = \tau(\sigma)$, so Equation 5 is non-linear. To solve analytically, the varying residence time would have to be condensed to an numerical function of coverage, in which case, the time needed to reach a certain coverage is:

$$t = \int_0^{\sigma} \frac{d\sigma'}{\alpha\phi - \dfrac{\sigma'}{\tau(\sigma')}} \tag{7}$$

This is assuming that there is zero coverage at time zero, $\sigma(t = 0)=0$. If we assume that the residence time is a step function, with a constant value for the 1st monolayer, then a smaller constant value for the 2nd monolayer, etc., then each step can be solved like in Equation 6. The time needed to complete the monolayer, assuming that conditions are right that equilibrium would exceed that monolayer, is:

$$t_{n+1} - t_n = \tau_{n+1} \ln\left(\frac{1 - \frac{\sigma_{n+1}}{\alpha\phi\tau_{n+1}}}{1 - \frac{\sigma_n}{\alpha\phi\tau_n}}\right) \tag{8}$$

As seen, there are only three parameters that affect the deposition level: the sticking coefficient, which determines what percentage of incoming molecules will become trapped on the surface, the impinging flux, and the residence time, which determines the average time that a "stuck" molecule spends on the surface. This project's objective desired to create a predictive model using as few inputs as possible, and has been narrowed down to four inputs: the substance and temperatures of the surface, the propellant substance, and also the partial pressure, or number density, of the propellant plume in the vicinity of the surface of interest and the following table relates how the inputs relate to these three parameters:

	α	ϕ	τ
Propellant substance	X	X	X
Surface substance	X		X
Surface Temperature	X		X
Prop. Partial Pressure		X	

Table 1. Model parameters and dependence.

1. Sticking Coefficient

The sticking coefficient is a complex characteristic that has to do with the energy required for a particle to avoid becoming trapped by a surface upon collision. In this manner, it is highly related to the accommodation coefficient. The well-depth potential of the surface that the gas molecule must overcome becomes stronger with decreasing surface temperature, and it obviously depends on what substance the surface consists of.

The other side of the interaction is the incoming gas molecule's energy, which, in macroscale, yields the gas mean temperature. Increasing the gas temperature increases the energy of the average molecule, which increases its chance of escaping the surface, thus, reducing the sticking coefficient. The sticking coefficient, in many papers, is only determined experimentally, and data are very scarce for cryogenic surface temperatures.[5] In fact, some have said that an analytic model does not exist.

Fortunately, at the low temperature of 40 K, the sticking coefficient for Argon, Krypton, and other heavy gases is cited between 0.7-1.0. For neon and hydrogen, it is usually cited anywhere between 0.1-0.7, while for helium, it is below 0.1. A paper by Goodman attempts to define the sticking coefficient as the fraction of a Maxwellian gas distribution that has energy above a "critical effective temperature".[6] A plot of g(t) gives the temperature distribution for a Maxwellian gas at mean temperature T_g.

$$g(t) = (1/T_g)\exp(-t/T_g) \tag{9}$$

where *t* is an "initial effective temperature", defined by,

$$t = MU_o^2 / 2k \tag{10}$$

where k is the Boltzmann constant, M is the atomic mass, and U_o is the initial speed of the gas, the sticking coefficient is simply the fraction of the gas atoms whose values of *t* are less than the critical temperature, t_c.

$$\alpha(t) = \int_0^{t_c} g(t)dt \tag{11}$$

It is simple up to here, but the math underlying his critical temperature is exceptionally complex, involving position and velocity response functions and other steps where the

values of parameters are not specified. At the end he produces a helpful theoretical plot for an impinging beam of noble gases on tungsten for surface temperatures ranging from 0-500 K. At 40 K his plot gives the following: Xe – 1.0; Kr – 1.0; Ar – 0.8; Ne – 0.1; He - < 0.01. The validity of his work is bolstered by experimental accommodation coefficient measurement data that very closely fits his own accommodation coefficient model plots.

The sticking coefficient should decrease slightly as the mean gas temperature is increased, indicating that the typical molecule has greater energy, as demonstrated in Equation 5. In our own work, trial tests were run with n-butane gas at 110-120 K to troubleshoot the experimental methods. The reason for this was that the QCM mass sensor would not operate below 90 K, until it was sent out for modifications and repairs. One test involved tracking the deposition rate at different gas temperatures with a constant gas flow rate. The sticking coefficient decreased from a value of 0.34 at 290 K, to 0.31 at 345 K. If lowering the equilibrium adsorption level by a small amount is critical, then raising the propellant exit temperature is one option (in the case of an electric thruster, raising the temperature of the escaping neutrals). But, it will be shown that the residence time is a much greater factor in the control of adsorption.

2. Flux

The impinging flux of surrounding molecules on a surface is typically calculated as:

$$\phi = \frac{n * \bar{v}}{4} = \frac{n}{4}\sqrt{\frac{8RT}{\pi M}} \tag{12}$$

with *n* and *v* signifying the number density of the gas and the average velocity of a gas molecule, respectively. This can be simplified for inputs of pressure P, temperature T, and molecular mass M. Of course, this is assuming an atmosphere of a constant pressure, such as in a vacuum chamber.

$$\phi = 3.513x10^{22} \frac{P(Torr)}{\sqrt{MT}} \frac{molecules}{cm^2 s} \tag{13}$$

3. Residence Time

The residence time was defined earlier in Equation 2. It represents the time that the average adsorbed particle will remain on the surface. The lattice constant, τ_o, is the time required for one vibration or oscillation of a surface lattice atom. It is the reciprocal value of the lattice oscillation frequency, and ranges from 10^{-12} to 10^{-14} sec. It is usually set at 10^{-13} sec, and will be here. The heat of adsorption, Q, is a function of the specific gas and material that it is in contact with, and the direct surface temperature dependence is clear. Determining the heat of adsorption is much more complicated than looking up a standard figure such as with the heat of vaporization, which is actually the heat of adsorption for a gas molecule upon a thick liquid layer of the same substance. Due to the exponential dependence on Q/T_s, the heat of adsorption has a huge impact on the residence time at 40 K, as shown in Table 2 for a sample gas with these heats of adsorption.

ΔH_{ads}	Residence Time
1.0 kJ/mol	$2.0x10^{-12}$ s
5.0 kJ/mol	$3.4x10^{-7}$ s
10.0 kJ/mol	1.14 s
15.0 kJ/mol	$3.9x10^{6}$ s
20.0 kJ/mol	$1.3x10^{13}$ s

Table 2. Residence times for various heats of adsorption at 40 K.

a. Derivation of the Heat of Adsorption

Determining the heat of adsorption ahead of time is the most difficult part of the project. It is a problem that appears on first glance to be much easier to approximate than in

reality. The heat of adsorption is simply a measure of the energy given up by a gas particle that becomes physically adsorbed on the surface. The heat of desorption is the amount of energy needed to break free of the surface, and is actually what we are interested in, but the two heats are basically identical. This energy is found by summing the interaction forces that bind a gas molecule to the atoms of the solid substrate. This is the same physical process as in condensation, except that the heat of adsorption refers to dissimilar particles interacting. For a gas molecule striking a liquid of the same substance, the energy is equal to the heat of vaporization, an important fact to keep in mind.

There are two types of intermolecular forces at play here, dispersion forces and electrostatic forces. Since we are mostly considering noble gas propellant, the electrostatic forces that generally apply to polar molecules are not very applicable here. The dispersion forces, also known as London or van der Waal forces stem from the temporary induced dipoles that come about whenever two atoms are close to each other. This is an attractive force that grows much stronger at close distances. In addition, there is a repulsive force that acts at very small distances arising from the interactions of the electron clouds of the two interacting atoms.[7] The two forces can be characterized by the Lennard-Jones potential, where the attractive term is definitely a 6^{th}-power dependence on distance, and the repulsive force is well-characterized by a 12^{th}-power dependence.

$$U_{VDW} = -\frac{A}{r^6} + \frac{B}{r^{12}} \tag{14}$$

When plotted, there is a minimum value where the potential is strongest. At this point, U_0, at a distance of r_0, the magnitude of repulsive force is generally 40-50% of the attractive force. The form of the L-J potential plot is shown below in Figure 4.

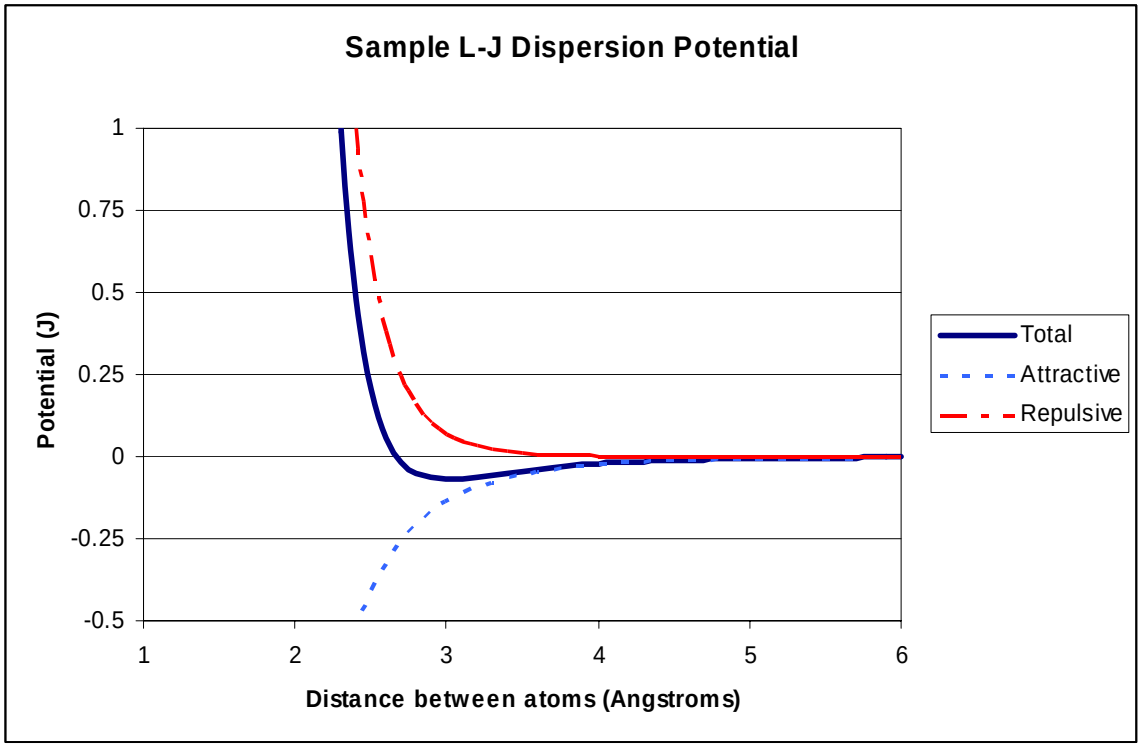

Figure 4. Example dispersion potential, r_0 = 3 Å

The A and B constants are empirical, although there are a couple of approximations out there. If it is assumed that at the equilibrium distance, r_0, the potential slope $d\phi/dr = 0$, then $B = Ar_0^6/2$. At this point, $\phi_{rep} = -0.5\phi_{att}$. One of the most commonly used approximations for A is the Kirkwood-Müller formula:

$$A = \frac{6mc^2\alpha_i\alpha_j}{(\alpha_i/\chi_i)+(\alpha_j/\chi_j)} \tag{15}$$

where m is the electron mass, c is the speed of light, α is the polarizability, and χ is the magnetic susceptibility, and i and j refer to the two interacting atoms or molecules.[8] One problem with this approximation is that the magnetic susceptibility is not constant with respect to temperature, which poses a problem since the TPF modeling is at 40 K, a region where susceptibility data are sparse, if they even exist. A more useful approximation in this case is the London approximation, where I is the first ionization energy:

$$A = \frac{3}{2}\alpha_i \alpha_j \frac{I_1 I_2}{I_1 + I_2} \tag{16}$$

The two *A* approximations were compared by calculating the heat of adsorption for cases that had been previously published. As it turns out, the Kirkwood-Müller formula was a good fit for the noble gases adsorbing on graphite[9], but it gave values much higher than those published for Argon and Krypton on platinum[10], and Xenon on nickel[11]. Conversely, the London approximation was about 10% higher than published data for Xenon on nickel, and about 7% low for Argon and 10% low for Krypton on a cryogenic platinum substrate (at 77 K for Ar, and 115 K for Kr). For graphite, the London approximation was far below the published results. Because the TPF craft uses a gold-plated substrate, and gold is next to platinum on the Periodic Table, as well as being a metal in general, the predictive model will use the London approximation for the *A* value.

The electrostatic interaction forces are important for polar molecules, but not as much for noble gases. This component has three separate attractive forces, the first is from an induced dipole from the electric field of the solid, the second is from a permanent dipole of polar molecules, and the third force is from a quadrupole moment. *F* is the electric field, *Fdot* is the field gradient, μ is the permanent dipole moment, θ is the angle between the field gradient and dipole/quadrupole axis, and *Q* is the linear quadrupole moment (positive or negative).

$$\phi_{elec} = -\frac{1}{2}\alpha F^2 - F\mu\cos\theta - \frac{1}{2}Q\dot{F} \tag{17}$$

The sum of the dispersion and electrostatic potentials gives the total energy needed for a molecule to break free from the surface at absolute zero. In addition, there is an additional unit of energy needed that comes from the heat energy of the substrate, which is cited anywhere from *RT/2* to *2RT* to *5RT/2*. For simplicity, the model will assume this is equal to *3RT/2*, which at only 40 K, is equal to the small amount 120 cal/mole. Thus,

the total energy required for desorption is assumed equal to the following (the dispersion and electrostatic potential are negative):

$$U_{des} = -U_{VDW} - U_{elec} + 120 cal/mole \qquad (18)$$

b. Heat of Adsorption Non-Idealities

In an ideal world, the test surface would be a perfectly smooth crystal face. The gas molecules would distribute themselves evenly, not interacting with each other, until full monolayer coverage was completed, then work would begin on the next layer, with interactions taking place between the gas molecules and the adsorbed layer of like molecules. (The term "monolayer" refers to a thin coating on a surface that is uniformly one atom or molecule thick.) In this case, the heat of adsorption with respect to surface coverage would be a step function, as in Figure 5. Unfortunately, even single-crystal structures have some flaws. The problem is that inside tiny cracks and pores, gas molecules are now in close proximity to more lattice atoms than on the surface, on more than just one side, and thus more tightly held. These "hot spots" tend to fill up first, so the heat of adsorption at very low coverage tends to be higher than for most of the initial monolayer. This behavior is shown in Figure 6.

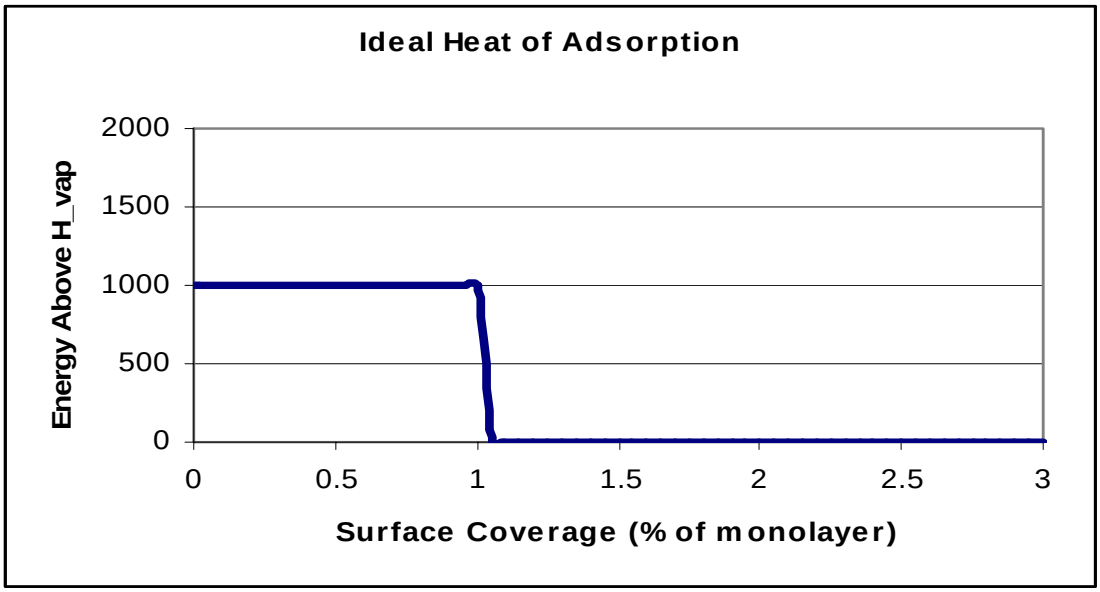

Figure 5. Ideal heat of adsorption with perfect surface, no adsorbate interactions.

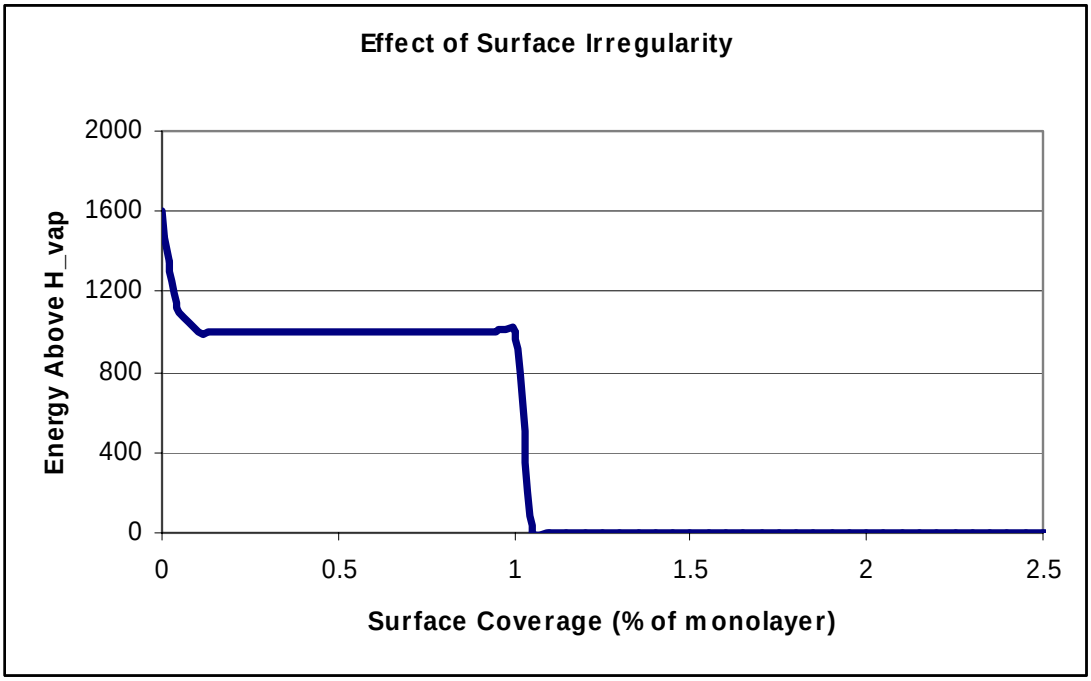

Figure 6. Surface irregularities, no adsorbate interactions.

Furthermore, the adsorbed gas molecules DO interact with each other, via the same dispersion forces that bond them to the surface. Thus, at low surface coverage, this can be neglected, but as the coverage increases past half of a monolayer, for any given layer, each gas particle is within reach of its neighbors, and the attractive forces hold them more

closely. This results in a rise of the heat of adsorption as the coverage approaches the monolayer or multilayer level, basically because the nearby gas molecules create shallow pits one atom deep that new molecules must sink into to bond with the lattice. This behavior is displayed in Figure 7. This behavior is partially, and sometimes totally, mitigated by the fact that impinging molecules do not completely fill a monolayer before starting on the next. What happens is that the second monolayer starts to fill up while bare spots remain on the lattice, just based on the chance positions that the gas molecules strike the surface. Since the heat of adsorption for a higher layer is always lower, this can negate the hump brought on by the adsorbate-adsorbate interactions.

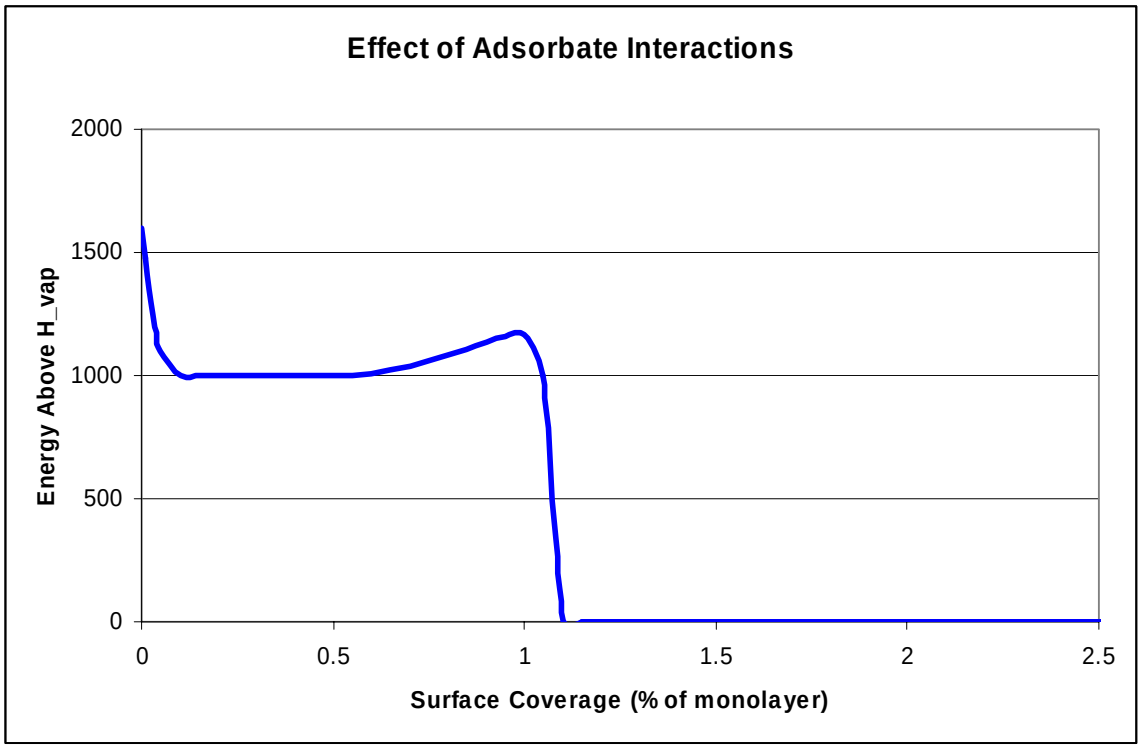

Figure 7. Heat of adsorption with adsorbate interactions.

Lastly, the lattice atoms continue to interact with adsorbate molecules above the first monolayer. One layer of separation is not enough to eliminate the dispersion force's pull between the surface and a new molecule. Chon's paper contains experimental data for the heat of adsorption of Argon and Krypton on a platinum substrate up to two monolayers. By about the 1.4 monolayer level where the surface irregularity effect has

diminished, the heats for Argon and Krypton are 1.138 and 1.137 times greater than their heats of vaporization, respectively.[10] Keep in mind that this represents a very clean surface. Thus, by the third and fourth monolayer, it can be expected that the required heat of desorption is equal to that gas's heat of vaporization. With a surface with pre-adsorbed atoms and other irregularities, it may take upwards of 10 monolayers or more to approach the heat of vaporization. The vaporization heats for Argon, Krypton, and Xenon are given in Table 3, along with the respective residence times for those gases' predicted heats at 40 K.

	Heat of Vap. (cal/mole)	**Residence Time (s)**
Argon	1538	2.71×10^{-5}
Krypton	2155	0.0656
Xenon	3015	3410

Table 3. Noble gas heats of vaporization and residence times.

From these data alone, Xenon is not a favorable choice for propellant if the flux is high, for reasons demonstrated in the next section having to do with the nearly 60-minute residence time. When all of these interactions and non-idealities are taken into consideration, the heat of adsorption vs. coverage plot becomes very difficult to accurately predict over a range of a couple of monolayers. However, the general shape shown in Figure 8 is expected to emerge when starting with a reasonably smooth and clean surface.

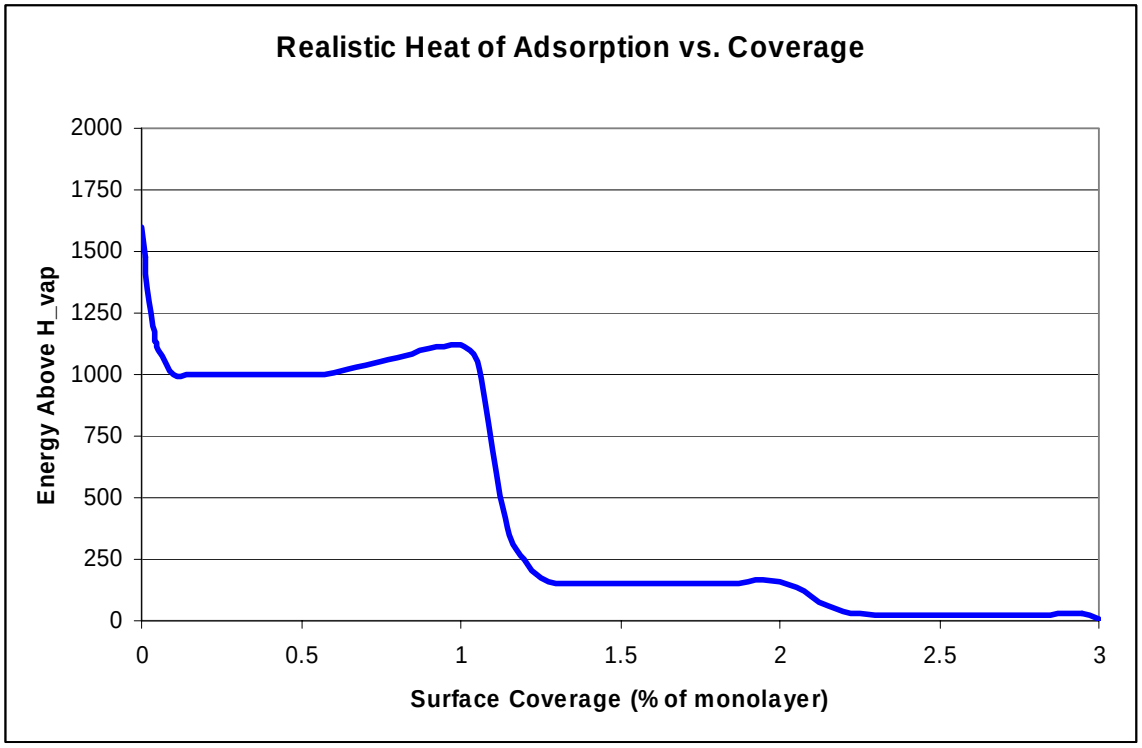

Figure 8. Realistic heat of adsorption vs. coverage behavior.

c. Applying the Heat of Adsorption to the Model

Determining the heat of adsorption by calculating the forces between a gas atom and a lattice atom would be reasonably easy if each atom only interacted with one surface atom. However, neighboring lattice atoms are in close enough proximity to exert enough force to demand consideration. For simplicity, it will be assumed that the substrate is arranged in a simple cubic pattern. In this pattern, there are three symmetrical spots where a gas atom could be absorbed. They are specified as A, B, and C in Figure 9. To calculate the estimated heat of adsorption, all of the lattice atoms will be considered within three multiples of the separation distance between two lattice atoms, d. Also, the gas atoms are assumed to float a distance of r_0 above the surface, which was defined earlier as the sum of the van der Waals radii of the two interacting atoms.

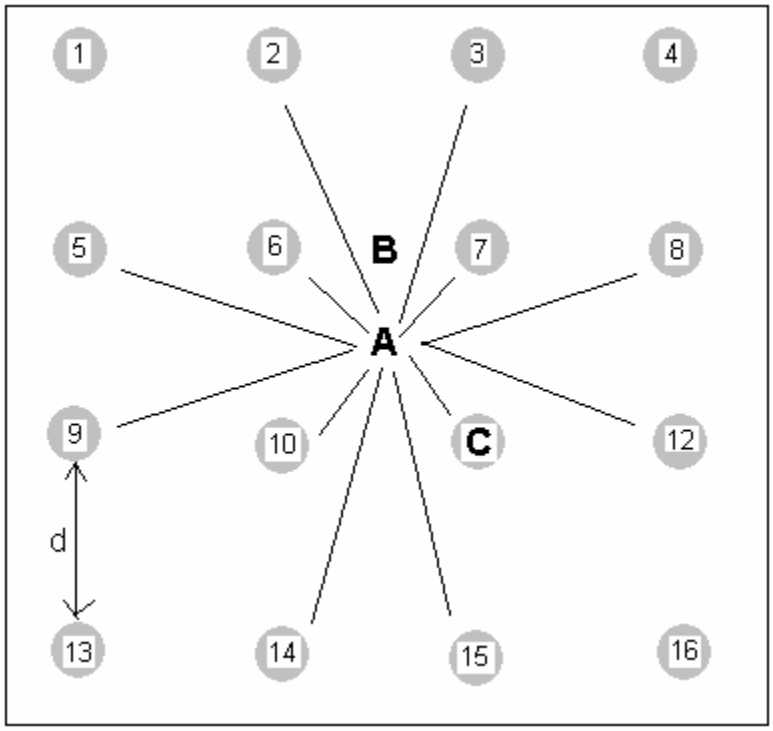

Figure 9. Cubic structure and allowed positions of gas atoms.

In this representation, all of the atoms within a distance of less than *2d* from **A** are assumed to interact with **A**. There are 12 lattice atoms within reach. For **B** there are 12 lattice atoms within reach (1, 2, 3…11, 12), and for **C** there are 9 atoms (6, 7, 8, 10, 11, 12, 14, 15, 16). This is within *2d*. In reality, all lattice atoms have an effect, but those beyond *4d* have a pull of under 5 cal/mole, and those beyond *5d* have a pull of less than 1 cal/mole. In addition, at these distances, there are atoms in lower layers of the lattice to worry about. For simplicity, all of those within 3d will be summed up, and an additional factor included for all beyond that distance. For a Xenon atom at position C, which is the easiest to model, on the top layer there are 24 atoms between *3d* and *4d*, and 24 between *4d* and *5d*. At *3.5d* the potential is equal to 9.0 cal/mole, and at *4.5d* the potential is equal to 1.9 cal/mol. Multiplying those average potential values by the number of atoms in those brackets give an additional potential of around 250 cal/mole for Xenon, 160 cal/mole for Krypton, and 110 cal/mole for Argon. The interactions are additive, so the potentials of the many interacting lattice atoms are summed up, which is added into A, B, and C. Since there will be twice as many **B** positions available as **A**'s or **C**'s, the gas-surface heat of adsorption is assumed to be:

$$U_{G-S} = \frac{U_A + 2U_B + U_C}{4} + 120 cal/mole \qquad (19)$$

The gas-surface potential values are as follows for the three gases in Table 4:

Gas	A	B	C	U_{G-S} (cal/mole)
Xenon	4090	3918	3795	**4050**
Krypton	3200	3096	3077	**3236**
Argon	2661	2535	2511	**2790**

Table 4. Estimated gas-surface potentials.

As the coverage approaches the monolayer level, the interactions with the fellow adsorbed adatoms must be taken into account. For simplicity, they will be assumed to adsorb at evenly spaced intervals in a cubic pattern, with a maximum density (coverage = 1.0) of the liquid plane density solved for in the next section. By taking the square root of the number of adsorbed atoms per unit area, the number of atoms/unit length can be found. The inverse value of this value will yield the average distance between adatoms. When the coverage is sufficient for this number to drop below *2d*, then an additional potential will be added to U_{G-S} consisting of the interactions with the four nearest adatoms. But, if incoming atoms strike already adsorbed molecules, they may begin the 2nd layer before fully completing the first, so this adsorbate-adsorbate potential will be assumed to be halved. Thus, for levels of coverage near monolayer completion:

$$U_{tot} = U_{G-S} + 4U_{G-G}/2; (r_g < 2d) \qquad (20)$$

To take into account surface irregularities, the heat of adsorption at zero coverage will be assumed to be 15% greater than U_{G-S}, and decreasing linearly down to U_{G-S} at coverage of 0.10 monolayers. The 15% factor was chosen because the TPF gold-plated mirrors are purportedly very smooth and regular. So, the modeled heat of adsorption will have the following profile:

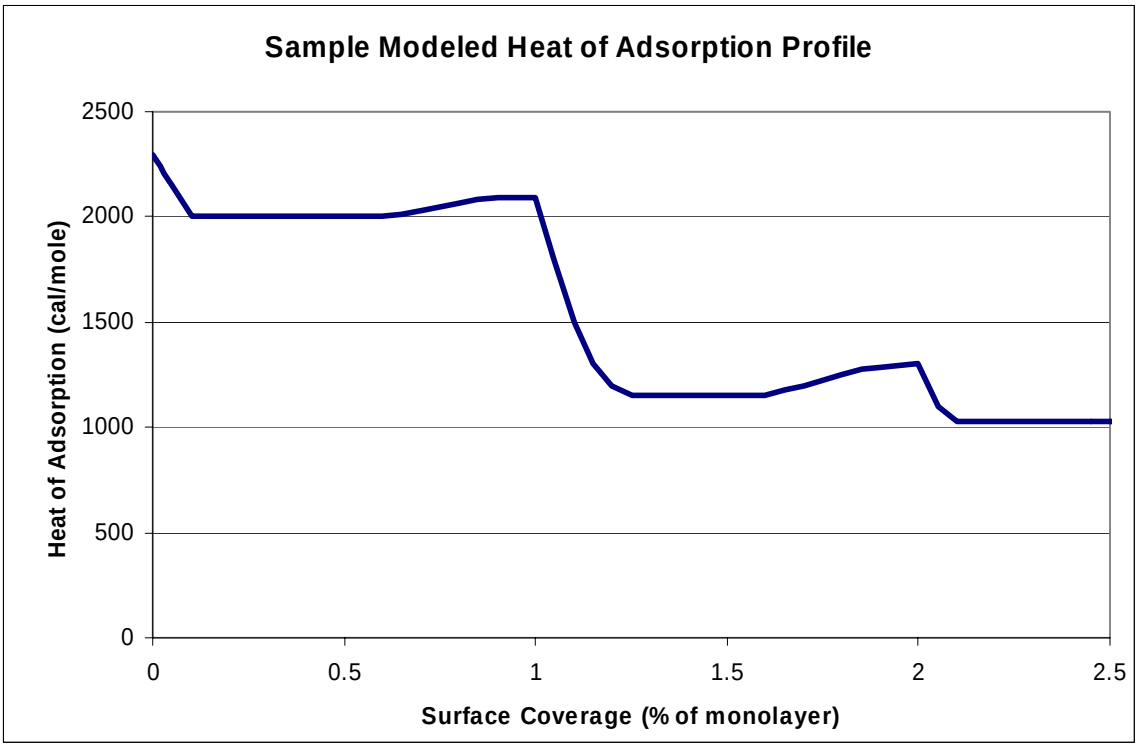

Figure 10. Modeled heat of adsorption, surface flaws and adatom interactions.

4. Density of a Monolayer

A monolayer is the proper baseline to consider because at this level of coverage, the deposition will probably have an effect on the optics. It is desirable to choose a combination of propulsion system, propellant, and surface temperature such that the equilibrium coverage does not surpass the one monolayer benchmark. This can be done.

The easiest way to calculate the number density of a monolayer for a given gas is to assume that the number of surface sites available for sticking corresponds to the number required for a liquid layer of the propellant. With this assumption, the value for liquid density can be divided by the mass of a single atom, in appropriate units, to yield the number density of a standard volume unit of liquid. Assuming that the atoms in the liquid cube would be arranged in a simple cubic packing form, the number density of one

face (monolayer) is the 3-D number density raised to the 2/3 power. The total calculation follows.

$$n_{2D} = \left(n_{3D}\right)^{\frac{2}{3}} = \left(\frac{\rho_{liquid}}{M(amu) * 1.66x10^{-24} \frac{g}{amu}} \right)^{\frac{2}{3}} \tag{21}$$

Table 5 uses Equation 21 to find the monolayer number densities for a number of possible propellant gases.

Propellant Gas	Monolayer Density (molecules/cm^2)
Xe	$5.833x10^{14}$
Kr	$6.704x10^{14}$
Ar	$7.618x10^{14}$

Table 5. Gas monolayer densities.

III. Model Predictions

A. Spreadsheet Setup

While the sticking coefficient and flux are important, they have only a linear effect on the total deposition. The residence time plays a much more vital role in determining the eventual equilibrium deposition level, as well as the time needed to reach that point, and the eventual time for the molecular coverage to desorb to a satisfactory degree. A spreadsheet was built that takes the surface and gas temperature, the sticking coefficient, the molecular mass and heat of adsorption of the gas, and the gas pressure as inputs. It outputs the flux and residence time, and calculates the deposition over a few hundred time steps, by recalculating the deposition rate at time step *t* using the total deposition of time step *t-1*, then multiplying that rate by the length of time between steps and adding the new deposition to that of the prior step. By setting the time step correctly, the deposition can be shown growing rapidly and then leveling off asymptotically. At the time of flow shutoff, the flux is set to zero, simulating the shutdown of the contributory thruster, and the deposition is allowed to evaporate for the duration of another few hundred time steps, depending on how much detail is needed. For the evaporative portion, the deposition rate equation simplifies:

$$\dot{\sigma} = -\sigma / \tau \tag{22}$$

If τ remains constant during evaporation, this integrates to:

$$\sigma = e^{-t/\tau} * \sigma(t_{flow\_off}) \tag{23}$$

By plotting a typical deposition scenario in log-linear space, one can see that the initial deposition rises rapidly to equilibrium, and desorbs logarithmically. In the case plotted

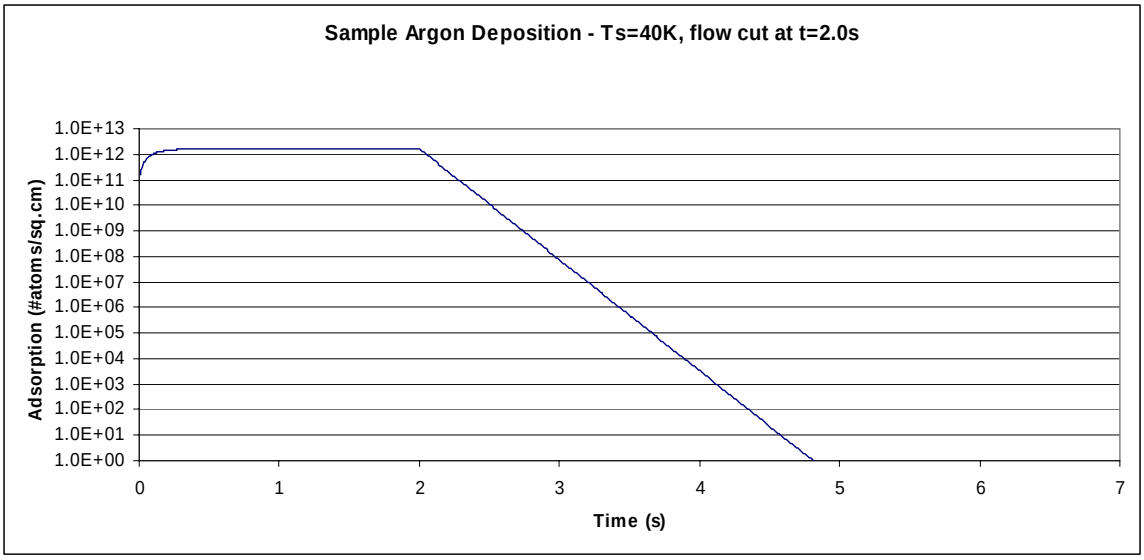

Figure 11. Sample plot of steady Argon flux, then turned off.

here, the gas is Argon, the surface temperature is 40 K, the gas temperature is 300 K, and the impinging flux corresponds to a partial pressure of 10^{-7} Torr. After two seconds, the flow is stopped, as if the surrounding space instantaneously became a total vacuum. The profile is shown in Figure 11.

In reality, the flux would drop to the ambient pressure of interplanetary space, which is on the order of 10^{-15} Torr, but the makeup of the ambient flux changes to the makeup of space, mostly hydrogen. Heavier gases typically will adsorb more easily. It is simple to calculate the time required to decrease the surface coverage by orders of magnitude, in multiples of the residence time. This is shown in Table 6.

Orders of Magnitude Reduction	Multiples of Residence Time
1	2.30
2	4.61
4	9.21
6	13.82
10	23.03

Table 6. Time required for deposition.

However, in the vacuum chamber, the base pressure is in the low 10^{-7} Torr range, although there is a hidden benefit to using cryogenic cooling. The pipes that bring the

liquid cryogen to the mass sensor become extremely chilled within minutes, to a much cooler temperature than the sensor, which has moderate thermal insulation. The pipe then acts as a crude cryopump, condensing the heavier gas molecules in the chamber and dropping the mean pressure to the 10^{-8} Torr level, although this more than likely is dominated by very light gases such as hydrogen and helium. The predicted deposition plot changes if the flow-off pressure is 10^{-8} Torr, and not zero. Thus, the desorption profile is expected to look more like that of Figure 12.

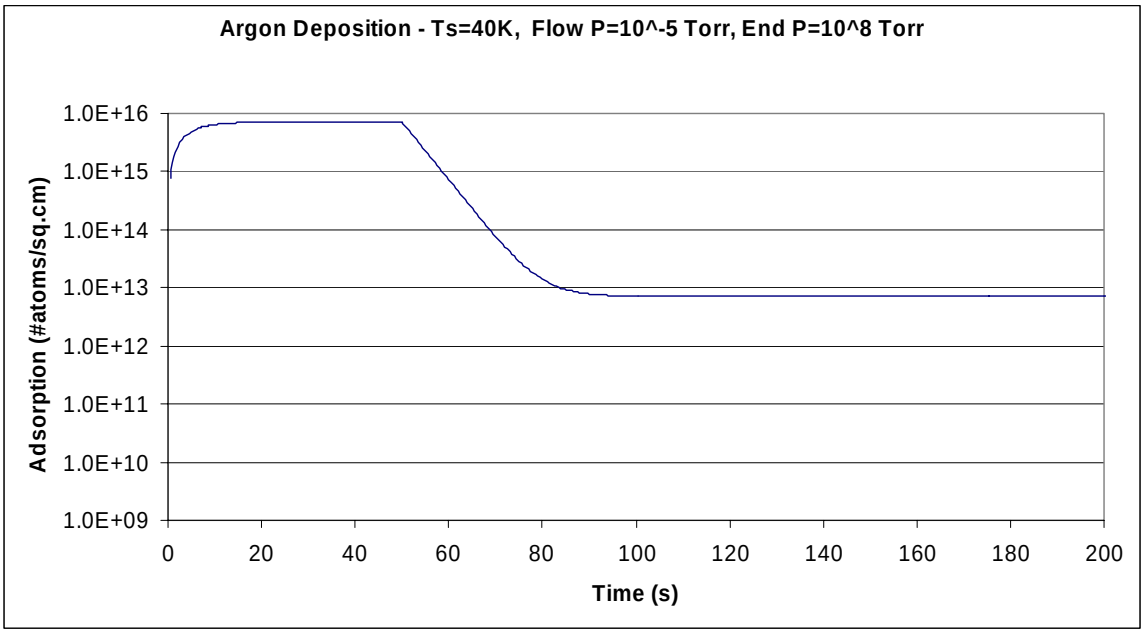

Figure 12. Model deposition profile with tank base pressure of 10^{-8} Torr.

B. TPF-specific Modeling

Through email conversations with John Treichler and Asif Ahmed, both of JPL, certain questions were cleared up. The 40 K temperature is a hard maximum for the mirrors, eliminating the possibility of raising the temperature by a few degrees to aid in desorption. It turns out that the bulk of the blackbody radiation emanating from the mirrors at any temperature higher than 40 K would fall in the range of near-infrared wavelengths that the interferometer is scanning for, corrupting the data. It was also confirmed that the

mirrors are gold-coated over a silicon carbide, or ultra low expansion (ULE) glass substrate.

1. Direct vs. Indirect Flux

When discussing the possible flux levels that the TPF mirrors may encounter, it is important to consider whether or not they are located in the line-of-sight of the thruster. When a surface is exposed to the plume, the direct flux is quite high – roughly a fraction of the of the total flux leaving the thruster equal to the ratio of the surface area to the total area that the plume has spread at that distance downstream. At the minimum TPF separation distance of 20 meters from center-to-center of adjacent satellites, there is a distance of about 10-12 meters from the thruster of one to the cooled mirrors of a neighbor. Fluxes of this variety and at this distance can be in the range of 10^9 – 10^{14} atoms/s/cm^2, depending on thruster selection.

Indirect flux refers to flux striking a surface from a thruster that can not be "seen". It involves atoms colliding in flight and being deflected towards the surface. In a weak vacuum this can be substantial as the background density is very high, leading to more collisions. In space, the background density is extremely low, so the indirect flux received by the surface will be lower by orders of magnitude, probably falling into the 10^6 – 10^9 atoms/s/cm^2 range or even lower. At this point it is uncertain what levels of flux are expected, or where the mirrors will be located, so it is necessary to model for a large range of fluxes. However, what if the expected flux turns out to be indirect and on the order of 10^6 atoms/s/cm^2? Then even for a theoretical gas with an infinite residence time (where nothing evaporates away), it would take more than a year to approach the monolayer level of deposition anyway, as there are 3.15×10^7 seconds in a year. If that is the case, an annual or semi-annual bake-out could remove any adsorbed real gas. An illustration of direct and indirect flux follows in Figure 13.

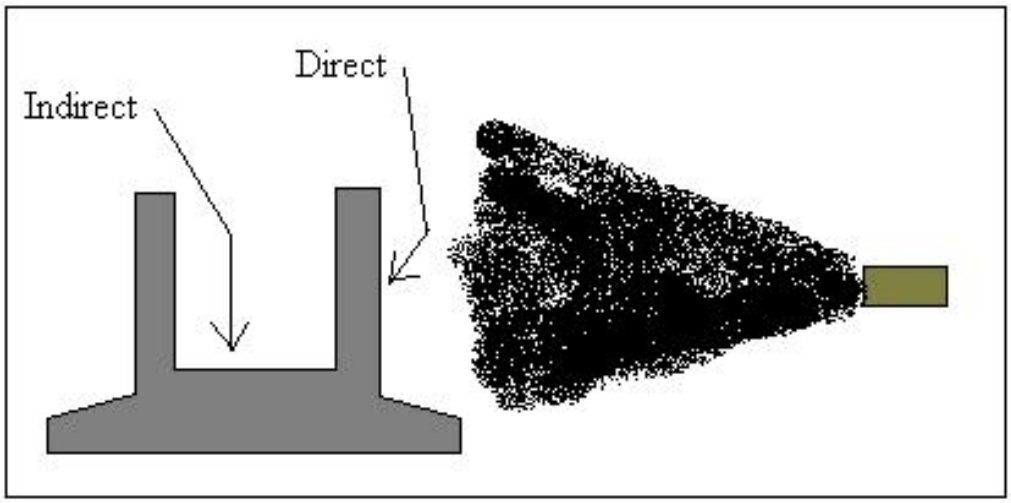

Figure 13. Direct vs. indirect flux

2. Pulsed Thrusters

Since the surface makeup and temperature are set, the major concern now is determining the average flux, as well as the firing patterns. The original TPF design plan called for a pulsed thrust approach, such as a PPT (Pulsed Plasma Thruster), which can run on different types of propellants. With this setup, the firing pattern to model would be a three-second window every thirty seconds during which the thrusters may fire. In reality, a PPT fires in microsecond bursts at very high levels of flux. But to model this pulsed thrusting scenario, the spreadsheet is setup with hundreds of thirty second-long time periods, with a lower constant flux on continuously for the first three seconds, to model what would be the worst-case-scenario: maximal thrusting, resulting in maximal flux. This flux can be seen as an averaged flux for the mass flow output for three seconds of PPT pulsed operation. The reason for having so many time periods is that for very low flux rates, it takes many periods to reach equilibrium. This may be the case with a low mass flow thruster impacting on a distant surface facing at an angle to its centerline.

When equilibrium is reached, there is a periodic oscillation every 30 seconds, where the deposition level rises rapidly for three seconds, then decays over the next 27 seconds back to the initial level at the start of the period. If the shutdown time is greater than the residence time, the peak deposition, at the end of the flux pulse will be equal to:

$$\sigma_{peak} = \alpha\phi\tau \frac{1 - e^{-t_1/\tau}}{1 - e^{-t_2/\tau}} \tag{24}$$

where t_1 is the time at shutoff (3 seconds) and t_2 is the time at the end of the period (30 seconds). If the shutdown time is much less than the residence time, the deposition will rise to a certain level, and then the oscillations will stabilize at specific amplitude. That behavior is shown in Figure 14. A simpler way to approximate the equilibrium deposition level is to determine the level of deposition where the adsorption rate, when the flux is on, is nine times greater than the desorption rate when the flux is off. Because the heat of adsorption changes as prescribed in Figure 10, the residence time changes, making this point more difficult to pin down analytically. It is easiest to just run the simulation for many periods until the deposition oscillations stabilize.

It is then possible to create a plot of equilibrium deposition versus flux for a specified gas-surface potential, $U_{G\text{-}S}$. The point used is the average of the peak and low point of the stable oscillations. Figure 15 shows a series of these plots on a logarithmic scale, corresponding to the estimated, low-coverage heats of adsorption ($U_{G\text{-}S}$ + 3RT/2) for Argon, Krypton, and Xenon, as provided in Table 3. It is important to note the upwards kink that occurs in all of the plots at a coverage of 10%. This is due to the way that the heat of adsorption is modeled (shown in Figure 10), at 10% coverage, it becomes constant until close to the monolayer level, and the residence time then becomes constant. Before that, as the coverage increased from 0.0% to 10%, the heat of adsorption and the residence time had been decreasing, which results in that leveling off behavior near 10% coverage.

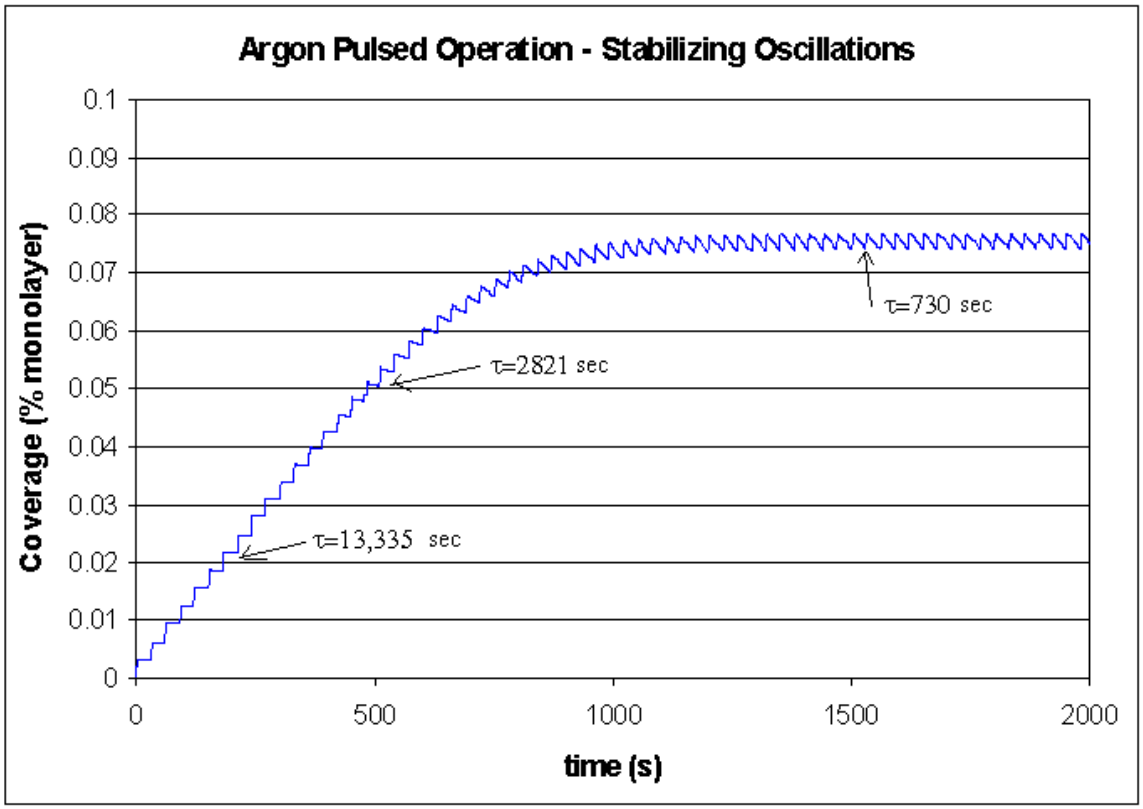

Figure 14. Equilibrium deposition behavior with pulsed thrusters

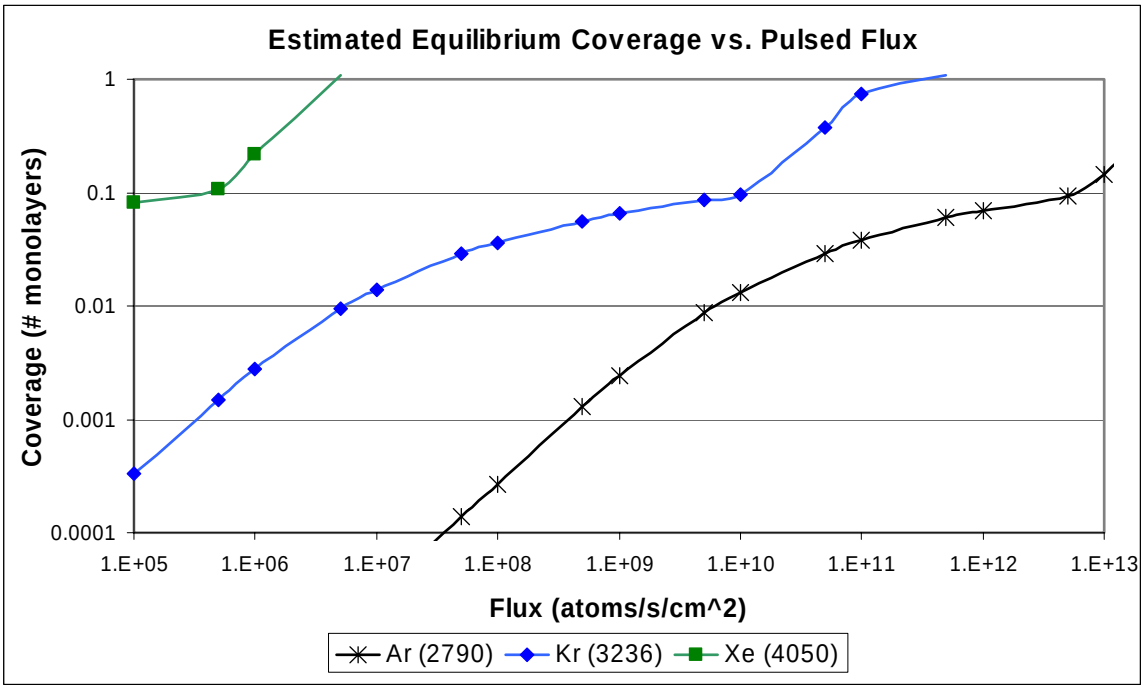

Figure 15. Equilibrium coverage for various heats of adsorption vs. pulsed flux

As shown on the graph, Xenon already exceeds the one-monolayer level before the flux reaches 10^7 atoms/cm^{2}s due to the high estimated heat of adsorption. At 40 K, it corresponds to a residence time of 50 years! Xenon performs slightly better for low levels of indirect flux, assuming that the predicted heat of adsorption is accurate. Krypton is predicted to do stay under 10% coverage until the flux = 10^{10} atoms/cm^{2}s, and performs well for indirect flux. Argon lags Krypton in deposition by a few orders of magnitude, making it a great choice up to very high level of flux. On the other hand, unless a multilayer deposition is acceptable, Xenon should be discouraged for all but very low flux situations. However, at this time, it is unknown where the acceptable coverage baseline lies.

3. Continuous Thrusters

At this time, the TPF propulsion group is considering the use of a continuous thrusting profile. More simply, they are considering a traditional ion engine that can be throttled for various levels of thrust. If a steady level of mass flow is assumed, this is an easier problem to model than that of the pulsed thruster. In this case, the equilibrium coverage is equal to $\alpha\phi\tau$, with the residence time changing due to the heat of adsorption's dependence on coverage, in accordance with Figure 10. The deposition profile would take the form of Figure 16.

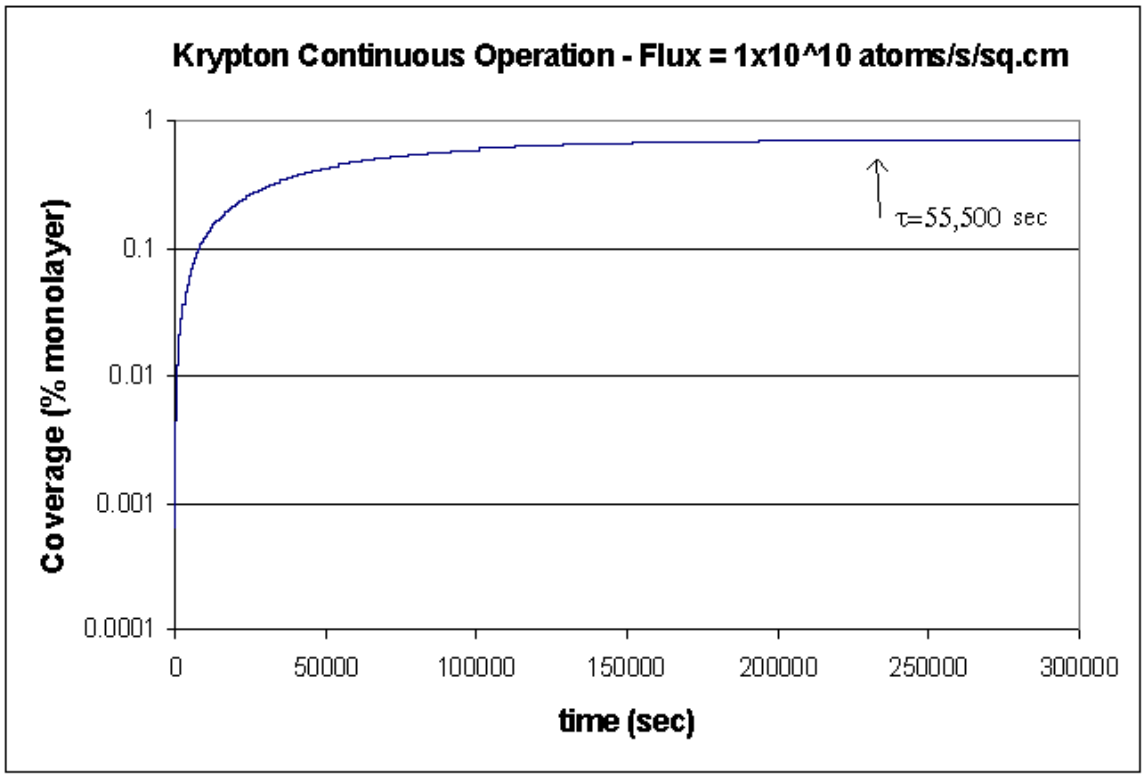

Figure 16. Sample deposition vs. time for continuous thrusting, constant flux

Similar to Figure 15, a plot of the estimated coverage levels for the three gases, as well as values 8-10% higher, are plotted in Figure 17 for continuously operating thrusters. In this scenario, Xenon will result in just over a monolayer of coverage at a flux of 10^6 atoms/s/cm^2, again, due to the colossal, 50-year residence time. Direct Xenon flux will certainly yield a multilayer coating of liquid Xenon. Krypton performs better, with 10% coverage at a flux of 10^9 atoms/s/cm^2, and for indirect flux, between 1% and 10% of a monolayer. Argon still performs excellently up to high direct levels of flux.

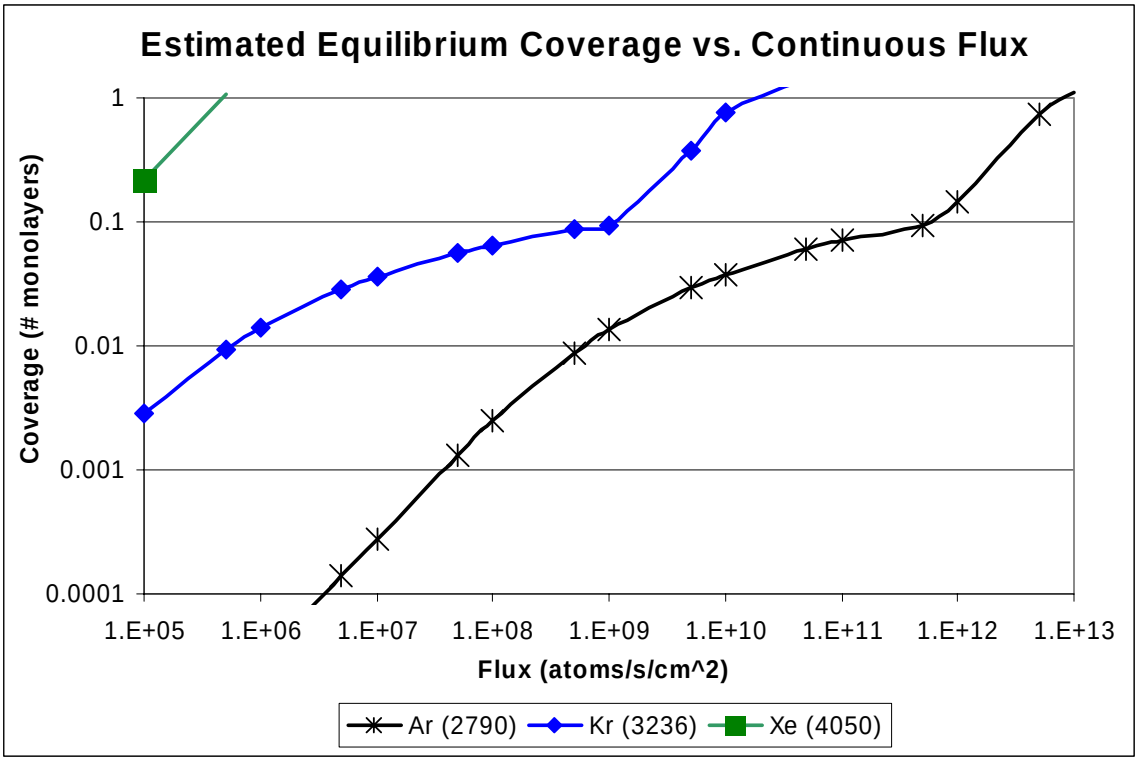

Figure 17. Equilibrium coverage for various heats of adsorption vs. continuous flux

4. Expected Thruster Flux

The thruster under consideration is the MiXI (Miniature Xenon Ion thruster). This thruster is a novel, very-low-power ion thruster, operating in a power range of 14-50 Watts, and producing 0.4-1.55 mN of thrust. At the point of optimal operating efficiency, the relevant parameters are as follows:[12]

Thrust	1.553 mN
Isp	3184 sec
Overall Efficiency	56%
Prop. Utilization	79%
Mass flow	0.050 mg/s

Table 7. MiXI characteristics

At a mass flow of 0.050 mg/s, the total flux is 2.28 x 10^{17} atoms/s. With a propellant utilization of 79%, the total ion flux is 1.80 x 10^{17} atoms/s, while the total neutral flux is 4.78 x 10^{16} atoms/s, with an average temperature of 280º C. At closest approach, the TPF satellites are 20 meters apart from center to center. Each satellite is estimated to be 15 meters wide, so the closest possible distance from a corner of the sunshield, where the thrusters are located, to the center of its neighbor, where the mirrors are located, is about 12 meters, although 10 meters will be assumed. Now using a simple assumption that the ion plume will have a divergence of 25º, the plume will spread from a 3cm diameter cross-section at the exit to a 468cm diameter cross-section 10 meters downstream. If the ions are evenly distributed in that cross-section, the downstream flux to a surface normal to the line of thrust is **2.618 x 10^{11} ions/s/cm^2** at 10 meters. For the neutrals, if they are assumed to spread evenly in a hemisphere from the exit, at 10 meters the flux normal to the discharge is **7.608x10^{9} atoms/s/cm^2**.

In comparison, a Busek model BHT-200 Hall thruster is considerably larger at 200 Watts, but still in the range of possible propulsion options. The BHT-200 is a Xenon-fueled thruster with a discharge voltage of 250 V and a total mass flow of 0.7 mg/s. Assuming the same plume divergence and propellant utilization of the MiXI, optimal operation results in an ion flux of **3.6x10^{12} ions/s/cm^2**, and a neutral flux of **1.0x10^{11} atoms/s/cm^2** at 10 meters downstream. The neutral flux is still fairly low. Figure 18 shows the ion plume divergence and neutral spread.

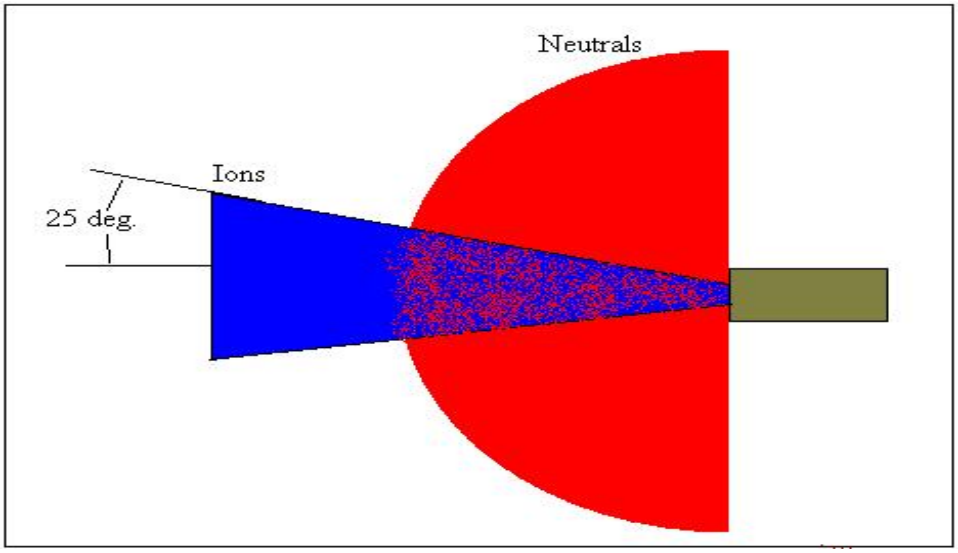

Figure 18. Ion and neutral downstream spreading

In reality, ion and neutral flows behave somewhat differently, but for simplicity and since it is not known whether or not the thrusters will fire towards the chilled mirrors, these crude approximations of flux suffice for direct flux approximations, within an order of magnitude. A real ion flux behaves as in Figure 19, which shows a BHT-200 Hall thruster plume 25cm downstream. In this plot, more than half of the flux is within 25º of the centerline, and over 90% is within 45º, so there is more divergence in reality.[13]

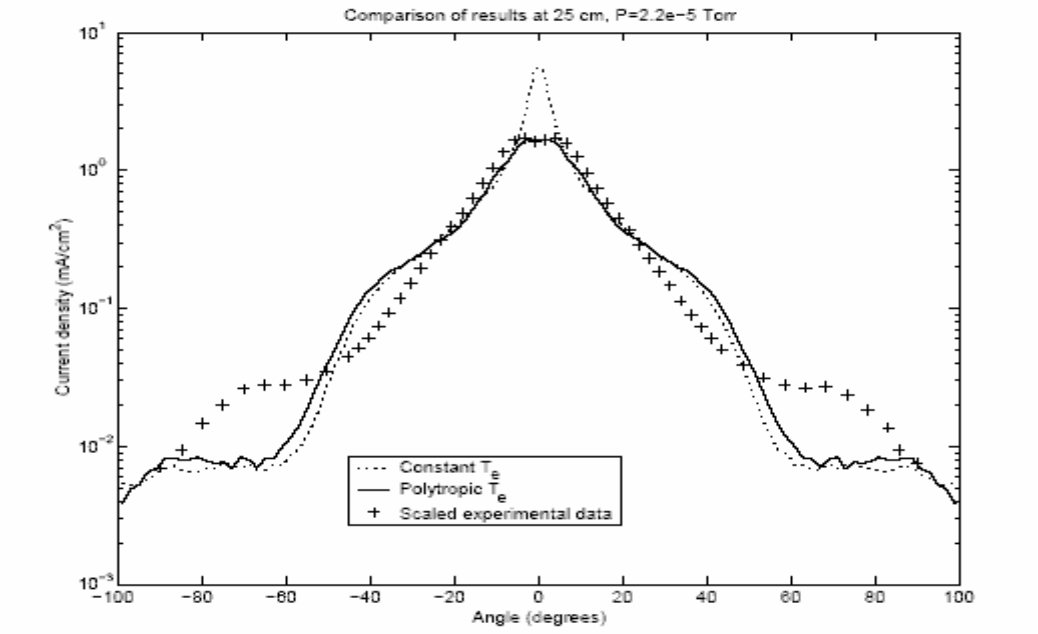

Figure 19. BHT-200 ion current density.

Neutral flow into vacuum is a well-understood problem, in this case, dealing with flow from an orifice into vacuum. Alexeenko provides helpful plots from micropropulsion research into orifice flow.[14] At 10m downstream in very high vacuum, the Knudsen number will be very high, *Kn >> 1*, so the flow will be mostly collisionless and will resemble the top half of the plot. The flow does not evenly distribute all the way out to 90º from the centerline, taking a lobe-shape, with most of the flux within 60-75º of the centerline. So, there is substantial neutral spreading, especially compared to ions.

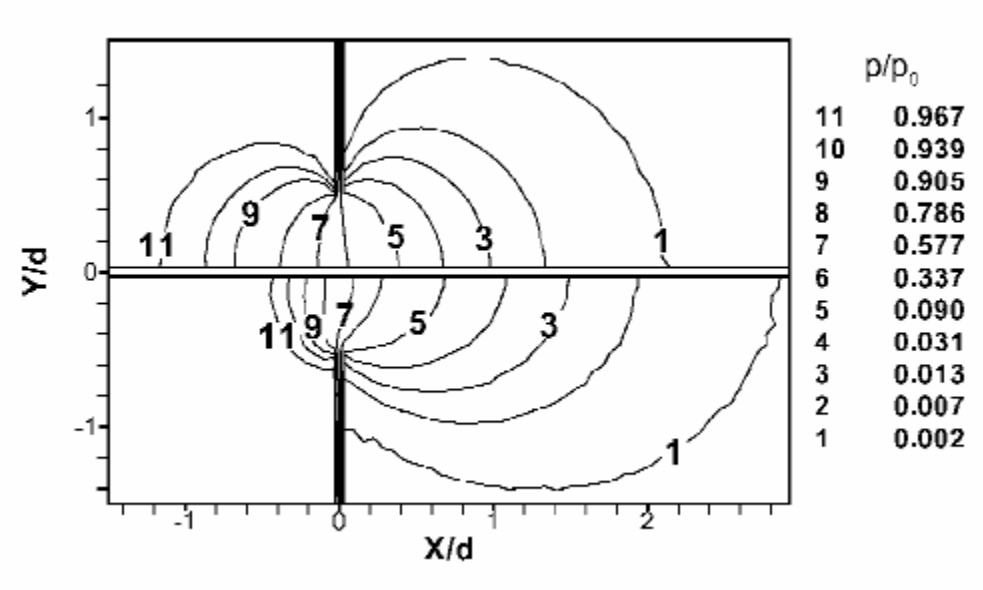

Figure 20. Neutral flow into vacuum from an orifice.

These flux figures look promising with respect to the predictions in Figure 14. Remember that these flux values are the highest possible fluxes that the sensitive mirrors would encounter from one neighboring thruster. These values assume the closest allowable proximity, continuous thrusting at the optimum point, and a surface normal to the line of thrust. Furthermore, published data by Ketsdever seems to suggest that the ion flux isn't even the main concern.[15] While discussing concerns of ground-based spacecraft-thruster interaction testing, he talks of the problems of high-energy ion sputtering in vacuum chambers. TRIM code shows that for Xenon ions with an energy of 400 eV, if they strike a Xenon-covered cryopanel surface at a glancing angle of 5º, they

will knock off an average of five adsorbed Xenon atoms. At a normal angle of 90º, an average of three Xenon atoms will be knocked off. The MiXI optimal point operates at a beam energy of 444 eV/ion. Even at sub-monolayer coverage, there is a good chance of an impinging ion knocking an adsorbed atom free, and even if it strikes a bare spot, with such a high energy, capture is unlikely, although there may be a danger of damaging the surface. Because of these factors, the neutral flux seems to be the larger concern.

IV. Experimental Setup

A. Motivation

Due to testing apparatus limitations, the decision was made to gather empirical data in a thruster-less setup. Since the final propulsion systems have not yet been selected, it is impossible to know what the plume conditions would be like tens of meters downstream. Because of that, a smaller thruster would need to be developed to produce the lower plume density within the depth of the SPL vacuum chamber. Also, with operational thrusters there is the issue of sputtered material, whether ceramic or metal, depositing on the QCM and corrupting the data. A thruster-less setup will therefore be considerably cleaner due to the lack of sputtered exit ring material.

Instead, a setup was chosen that allowed more flexibility in gas selection, temperature, and particle density. A mass sensor is mounted inside of a small vacuum chamber, while gas is leaked in. A valve controls the gas flow, and hence, the pressure inside the chamber. The incoming gas can be heated up to 100 K above room temperature, by heating the chamber walls. A copper coil is wrapped around the mass sensor, and cryogenic liquid flows through the coil, allowing the sensor to attain the low temperatures needed to simulate conditions that will be encountered by the TPF spacecraft. A schematic is shown in Figure 21.

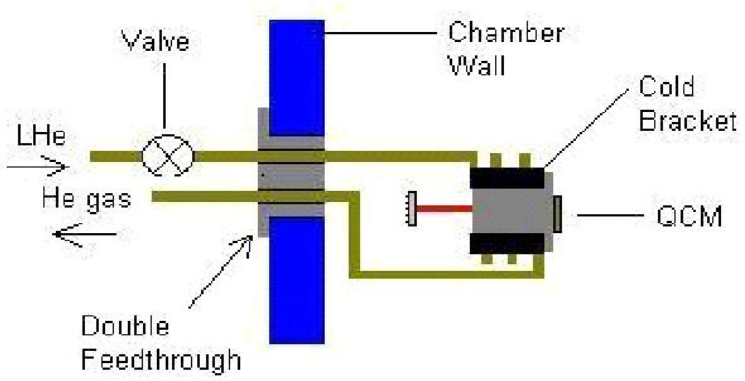

Figure 21. Experimental setup schematic.

B. Equipment

A model MK16 quartz crystal microbalance (QCM), acquired from QCM Research, is used as a mass sensor and is mounted inside of a small vacuum chamber. This chamber is equipped with two Varian V-70 turbopumps, capable of producing pressures in the 10^{-7} Torr range. The chamber setup requires three feedthroughs, all purchased from MHC. One is for a 9-pin D-type double male connector, for connecting the QCM to the M2000 data acquisition unit, also from QCM Research. The second feedthrough is used to allow the atmospheric gas into the chamber. It has a tube running through it with ¼" Swagelok male connectors on each end. The tank end is left open, while the outside end is connected to a capillary line that leads to an Upchurch-brand micrometering valve. This valve regulates the flow from the atmospheric gas bottle, and allows more precise control than a standard gas bottle regulator. The third feedthrough is a ¼" double fluid feedthrough, with both internal ends connected to a custom-made copper coil surrounding the QCM bracket.

C. QCM Theory

A quartz crystal microbalance measures mass by comparing the resonance frequency of two matched crystals. One is tucked inside the QCM as a reference crystal, and the other is exposed to the outside. The exposed crystal's frequency decreases with any additional mass per unit area ($\Delta m/A$) that accumulates on the exposed face. The output signal, F, is simply the difference between the reference and exposed crystals. Thus, with increasing deposition, the resonance frequency of the exposed crystal will decrease, and the signal will increase:

$$\Delta F = S_f * \frac{\Delta m}{A} = S_f * \rho * \Delta \tau = S_f * \rho * \delta * \Delta t \qquad (25)$$

S_f is the crystal sensitivity factor, ρ is the density of the deposited material, $\Delta\tau$ is the deposition thickness, and δ is the deposition rate. For the model MK16 CQCM that was used, S_f = 5.0917 x 10^8 Hz*cm^2/g. The diameter of the crystal surface is ¼", so the area works out to 0.317 cm^2. The MK16 is shown in Figure 22.

By inverting the sensitivity factor, the QCM can be characterized by how small of a mass can be measured. Each frequency rise of 1 Hz corresponds to a deposition of 1.963 x 10^{-9} g/cm^2. The area of the crystal surface is 0.317 cm^2, so the total mass increase per 1 Hz rise is 6.226 x 10^{-10} g. In accordance with the monolayer densities given in Table 4, the coverages that can be measured with the MK16 are as follows in Table 8. Furthermore, the QCM is rather accurate down to 0.1 Hz which can increase the resolution by an order of magnitude, provided that the temperature is very stable, not rising or dropping at all.

Gas	***Atoms/cm2***	***% Monolayer***
Xenon	$9.02x10^{12}$	1.55 %
Krypton	$1.42x10^{13}$	2.12 %
Argon	$2.95x10^{13}$	3.87 %

Table 8. Coverages for a 1 Hz increase in QCM freq.

A QCM from QCM Research can come in one of two temperature types, a standard model, and a more expensive cryogenic-rated model. The CQCM requires a different set of internal hardware, but can function accurately down to 10 K, whereas the standard temperature models become unreliable around 90 K. The maximum operating temperature for both types is 400 K. In addition, there are two methods of temperature control offered. The TQCMs (Thermoelectrically-cooled QCM) use a Peltier cell to heat or cool the crystals. The CQCMs, including the MK16 used for this project, contain an internal heater, but require an external heat sink to be attached to the case of the QCM. They must be cooled below the desired crystal temperature for the heater to control the temperature, as it can only add heat in varying intensities to offset the energy lost to the heat sink.

Figure 22. MK16 CQCM model.

D. Cooling Circuit

The cooling circuit consists of eight components. Most important are the dewars of cryogenic fluid, both liquid nitrogen (LN) and liquid helium (LHe), which are procured from the MIT Cryogenics Lab. On the first test run with LHe, it took over two hours to cool the QCM from 290K to 95K. This is due to the fact that the QCM sensing crystal is heavily thermally insulated. LHe is quite expensive at $4.50 per liter, while cooling runs through about 5L/hour. LN, on the other hand, sells for about 20 cents per liter. Unfortunately, the cooling can not be done with nitrogen down to 100 K, and then switching to helium for the rest because the initial rush of warm helium gas through the coolant pipes warms them up briefly, releasing anything that had condensed on them. Instead, liquid nitrogen is used to cool down the coolant feedthrough, by wrapping a 1/8" copper coil around the feedthrough and flowing LN. This was suspected as a heat source that was warming up the liquid helium, so dropping the surface temperature of the chamber in the vicinity of the feedthrough should reduce the heat flow to the helium.

Liquid nitrogen and helium have different insulation needs, and thus, different connection systems. A short copper connector pipe was made to connect the LN dewar to the cooling coil around the double feedthrough. The LHe dewar requires a vacuum-insulated transfer tube. The MIT TELAC group had such a transfer tube and lent it to the TPF team. The apparatus is shaped like a U, with a long thin pipe on one end that descends into the liquid helium. The other end is a straight length of vacuum insulated tube with a

5/8” threaded ending. The two tubes are connected by stainless steel, flexible vacuum tube. A stainless steel adapter was machined to connect the threaded end and the Swagelok fitting on the feedthrough. Pictures of the copper connector, double feedthrough, and adapter are shown in Figure 23.

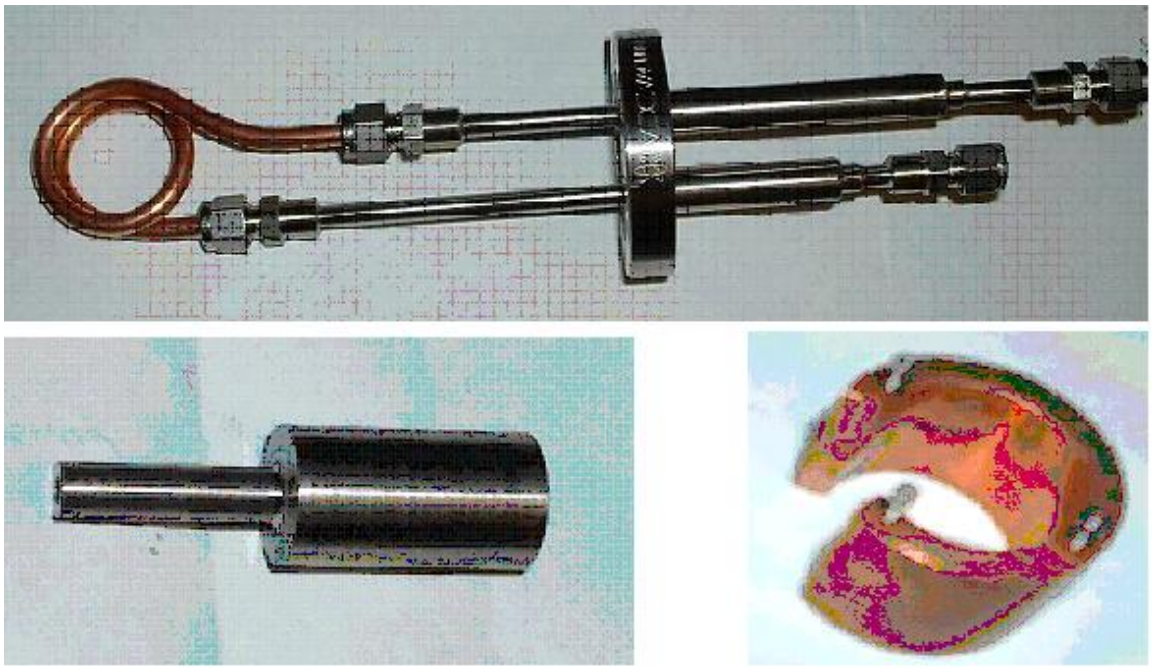

Figure 23. Feedthrough/coil (top), adapter (left), QCM connector (right).

A view inside the chamber in Figure 24 shows the QCM, and the machined copper bracket that it is fastened to.. The bracket is meant as a heat conductor, or in this case, a cold conductor. A coil of ¼” copper tube is wrapped around the bracket and connected to both inner ends of the double feedthrough. The liquid cryogen flows from the dewar, through the coil, and back out of the chamber. The high heat conductivity of copper ensures that the coil and bracket will get sufficiently cold enough to sap heat away from the case of the QCM – the only way to cool the inner insulated crystals. With liquid helium flowing, the QCM outer case cools to 50K in less than 10 minutes, as verified by a thermocouple, and the sensing crystal reaches an eventual temperature of 60-62K after approximately three or four hours of cooling.

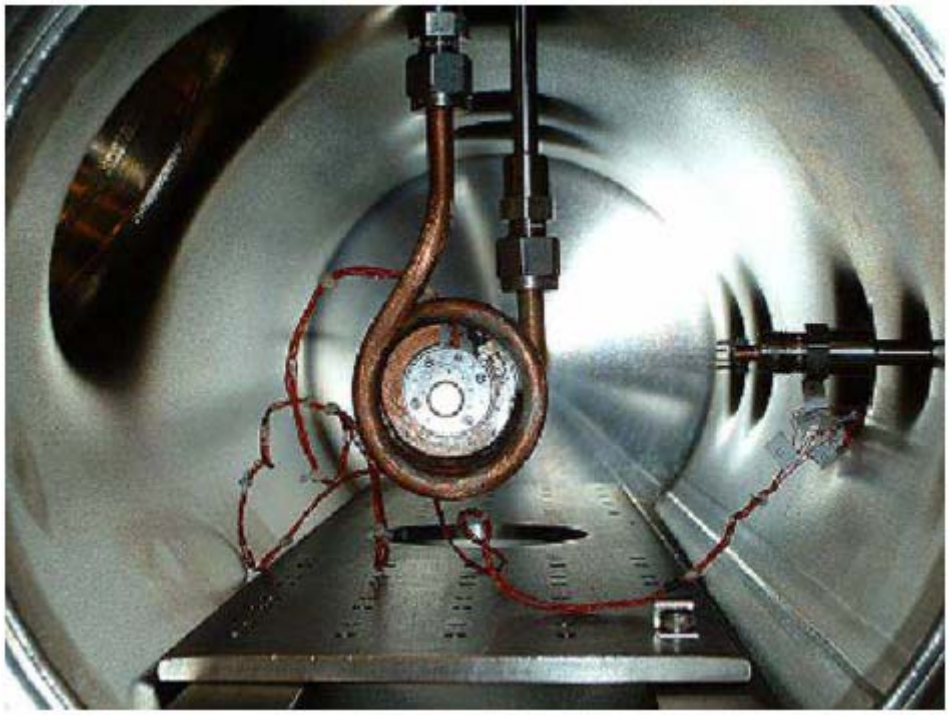

Figure 24. Inside the vacuum chamber.

Connecting to the outside output of the double feedthrough is a foam-insulated, bent copper tube that extends from the vacuum chamber into a fume hood. The used cryogenic fluid, now a gas, is expelled into the hood. A picture of the entire setup from the outside is displayed in Figure 25.

Figure 25. Overall view.

V. Testing

Since the monolayer densities have been approximated, the model can be used to simulate the peak deposition levels in terms of fractional surface coverage, with 1 monolayer = 100%, for any set of gases and conditions, provided that certain characteristic properties are known. In addition, the fractional surface coverage can be used to change the heat of adsorption in accordance with Figure 10. As it turns out, the residence time, because of the heat of adsorption, is the driving factor in determining not only the eventual surface coverage but also the time needed to evaporate down to a maximum desired level of coverage. As shown in Equation 2, there is an exponential dependence on the heat of adsorption and an inverse exponential dependence on the surface temperature. A small change in either term can have a large impact on the residence time.

For the temperature they must be kept at, the TPF mirrors are almost an ideal surface for minimizing adsorption, as they are homogenous and very smooth. Predicting the adsorption and subsequent desorption after encountering a flux of propellant particles is easier for this ideal surface than for the QCM. The TPF craft is in the hard vacuum of space, where interactions with stray atoms and molecules are orders of magnitude lower than in a vacuum chamber with a base pressure of 10^{-8} Torr. There is a much higher chance of water vapor or oxygen or carbon dioxide molecules adsorbing to the crystal face during the cooldown process before the atmospheric gas is even introduced. To lessen this impact, the QCM can be heated above room temperature when the coolant is first turned on. The cooling circuit pipes cool down to below 100 K in minutes and act as a crude cryopump, whereas the QCM is thermally isolated, taking much longer for the crystal to cool. When that happens, the heavier molecules should adsorb onto the pipe for the duration of the test, and pre-heating the crystal will help to evaporate whatever is already adsorbed. But, this is not perfect, so the surface is not expected to be as smooth, resulting in a higher heat of adsorption during the tests. How much higher is simply

guessing. In addition, any deposition of sputtered material from past tests would most likely remain on the surface.

One benefit to having a slightly occluded crystal surface is that for whatever heats of adsorption are measured, the actual TPF performance will certainly be better. As for the vacuum chamber tests, there are two ways in which to determine the heat of adsorption.

1. The heat of adsorption can be found by leaking in a constant supply of test gas into the chamber, stabilizing the pressure to yield a constant flux, and waiting for the deposition to flatten out to an equilibrium level. At this point, the deposition level is equal to the product of the sticking coefficient, the flux, and the residence time (Equation 1). The residence time is the only unknown in this situation, and when found, the heat of adsorption can be obtained. At very low temperatures, the sticking coefficient will be very close to 1.0, but it can be verified by running a steady-flux test at a lower temperature, where the residence time is very high, and the deposition rate is equal to $\alpha\phi$. When searching for an equilibrium level, the choice of surface temperature is very critical. If the temperature is a little too low, the residence time will be too high, and deposition will be well over a monolayer, possibly into full condensation. If the temperature is too high, the equilibrium point may be too low to be measured accurately. The ideal level is between 0.2 and 0.8 monolayers.

2. If a gas flow is supplied such that deposition builds up past the one-monolayer level, it can then be shut off, and the adsorbed material will desorb from the surface at a rate equal to $-\sigma/\tau$. This results in an exponential decline of the total number of adsorbed atoms via Equation 23. The residence time can be found which leads to the heat of adsorption. Here again, the surface temperature is critical, because it sets the residence time for a given heat of adsorption. This exponential decline only applies while the residence time is constant. If you start from a thick layer, the residence time will vary significantly as the coverage decreases during evaporation. You can track $ln(\sigma)$, and at each coverage,

$$\tau(\sigma) = \left(\frac{d \ln \sigma}{dt}\right)^{-1} \tag{26}$$

Because of the changing residence time, it is advisable only to focus on a small range of coverage for each test. In order to get enough data points to accurately fit the data, the residence time should be greater than 10 seconds, but if it is too high (above a few minutes), desorption will take too long, and signal drift could corrupt the data. Ideally, residence times should be in the 30-180 second range. Due to the slow data collection rate of the QCM, this method is ill-suited for the setup being used for this work, but is a useful method with more precise equipment.

To find the heat of adsorption using these two methods, the temperature must be controlled very precisely. The tests are conducted at intervals of a few Kelvin when residence times and equilibrium coverage levels are in the desired ranges. The values of the heat that result from this testing will be used to hopefully verify the model, and if they prove to be far off from predictions, then they will serve to troubleshoot the model. Regardless, what the data shows for a gas adsorbing on the gold-plated QCM under vacuum should well represent what will transpire between that gas and the gold-plated mirrors of the TPF craft in the vacuum of space.

VI. Testing Results and Analysis

A. Testing Conditions

Data were collected for Xenon and Krypton at several different temperatures and several different pressures for each temperature. Due to the extreme sensitivity of the micrometering valve, attaining the same pressure each time is quite difficult. The smallest turn of the valve can increase the pressure by 15% or more, especially at the low end of the attainable pressure range. But, since the residence time changes with surface temperature, the same fluxes will produce different levels of coverage at different temperatures. In some cases, identical coverage levels are attained at two temperatures, but this is due to luck more than design.

For Xenon, data were taken at 5 temperatures: 65 K, 68 K, 70 K, 72 K, and 75 K. The pressures tested are listed below in Table 9.

65K	68K	70K	72K	75K
3.0×10^{-9}	2.0×10^{-8}	2.1×10^{-8}	1.0×10^{-7}	5.1×10^{-8}
7.4×10^{-9}	1.0×10^{-7}	6.7×10^{-8}	3.5×10^{-7}	1.0×10^{-7}
2.1×10^{-8}	5.3×10^{-7}	4.5×10^{-7}	1.2×10^{-6}	5.1×10^{-7}
1.3×10^{-7}	1.3×10^{-6}	1.3×10^{-6}	5.0×10^{-6}	1.0×10^{-6}
4.6×10^{-7}	2.5×10^{-6}	6.0×10^{-6}		3.4×10^{-6}
6.8×10^{-7}	4.5×10^{-6}			
1.1×10^{-6}				

Table 9. Xenon test condition pressures, in Torr.

For Krypton, data were taken at 3 temperatures: 65 K, 66 K, and 68 K. The cooling circuit would not go below 64.5 K during the Krypton testing phase, without precipitous helium flow rates that would quick drain the dewar. The pressures tested are listed below in Table 10.

65 K	66 K	68 K
5.1×10^{-8}	3.6×10^{-8}	3.1×10^{-8}
9.5×10^{-8}	8.9×10^{-8}	6.7×10^{-8}
2.3×10^{-7}	2.4×10^{-7}	1.0×10^{-7}
4.6×10^{-7}	4.2×10^{-7}	3.1×10^{-7}
7.5×10^{-7}	7.9×10^{-7}	5.6×10^{-7}
1.4×10^{-6}	1.3×10^{-6}	7.9×10^{-7}
	2.0×10^{-6}	1.3×10^{-6}
	4.0×10^{-6}	2.3×10^{-6}
		3.1×10^{-6}
		5.0×10^{-6}

Table 10. Krypton test condition pressures, in Torr.

B. Data Reduction Process

As explained at the end of Chapter V., the method best suited for this experimental setup is to turn a steady flux on until equilibrium coverage is reached. The residence time can be found in accordance with Equation 1. The sticking coefficient will be assumed to be 0.9, in accordance with Goodman's data[6], and the flux is solved for with Equation 13, leaving only the residence time as an unknown. The frequency rise corresponding to the increased deposition is converted into coverage by the factors listed in Table 8. The coverage is easily converted into atoms/area by multiplying by the monolayer densities estimated in Table 5. Now the residence time can be found. Once found, the surface temperature is known, so Equations 1 and 2 can be rearranged to solve directly for the heat of adsorption. In this case, solving for Xenon where a frequency rise of 1 Hz corresponds to a deposition of 9.02×10^{12} atoms/cm^2.

$$Q = RT_s \ln\left(\frac{\Delta F * 9.02 * 10^{12}}{\tau_o \alpha \phi}\right) \tag{27}$$

Precisely determining the frequency shift is a slightly more difficult problem because there is a steady signal drift in the QCM readings of about 3.0-3.5Hz/min, and a steady rise once equilibrium is reached. This second rise only occurs when the gas is flowing,

and is directly proportional to the gas flow rate, most likely pointing to an impurity in the gas supply. Once the flow is cut off, the gas desorbs, leaving a base frequency that is higher by the amount attributable to this impurity rise. Figure 26 shows an untreated plot, then when the signal drift is canceled out, and also with the impurity rise canceled out. Here, the frequency rise is about 38 Hz for the version used for analysis, which is the plot with the drift and impurity canceled out. .

For this particular data point, the frequency rise is about 38 Hz, which corresponds to 58.9% coverage. At a pressure of 1.3 x 10^{-7} Torr, the flux is 2.30 x 10^{12} atoms/cm^2. With an assumed sticking coefficient of 0.9, the residence time is 16.6 seconds, which yields a heat of adsorption of 4214 cal/mole.

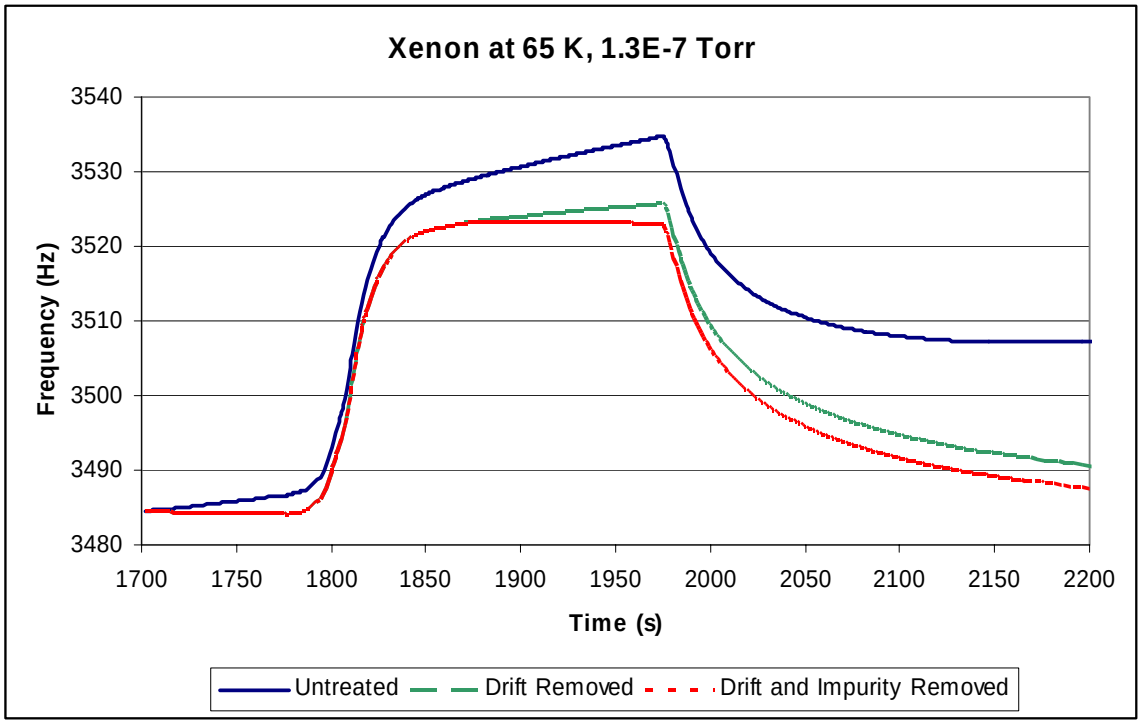

Figure 26. Xenon plot showing raw data and treated data.

C. Errors

With a setup such as the one used here, there are bound to be some inaccuracies that come into play. The possible inaccuracies are in the pressure measurement, the frequency measurement, the surface temperature measurement, and in the sticking coefficient assumption.

The pressure gauge is a cold cathode gauge that is rated to be accurate +/- 5%. In addition to that specification, it differs slightly from a filament gauge installed in the vacuum chamber. One or the other may be out of calibration, so the pressure reading will be assumed to be subject to a +/- 10% error. The QCM was just calibrated and had a new silicon diode temperature sensor installed before being used for this testing, so the frequency and crystal temperature should be highly accurate, within +/- 0.1 Hz on the frequency and +/- 0.05 Kelvin. At the frequencies and temperatures tested, those errors are less than 1% of the values attained for frequency and temperature (a 3500 Hz reading and ~70 K). As for the sticking coefficient, the Goodman paper gives an estimate of 0.99-1.0 for Xenon around 70 K, and about 0.9 for Krypton at 70 K on tungsten. Because I have not found any other data of the sort, I will assume a +/-10% error for the sticking coefficient, allowing it to vary from 0.8 to 1.0, although it will be modeled as 0.9. Lastly, canceling out the drift and impurity frequency shifts may affect the accuracy of the frequency difference by 0.5 - 1.0 Hz or so, with is generally <5% of the total coverage.

Pressure and the sticking coefficient linearly affect the coverage and the residence time. However, the heat of adsorption is in an exponential, so while the total error allowance of +/- 25% seems high, it has a much lower effect on the heat. For the example in Figure 26, the maximum 25% increase or decrease in the residence time gives heat of adsorption error bars of between **4186** cal/mole and **4251** cal/mole on a measured value of **4214** cal/mole, which amounts to about a +/- 0.8% error in the heat of adsorption value. For Krypton, the error bars will be set at +/- 1.0%, because the primary impurity in a Krypton gas bottle is Xenon, which will certainly stick when Krypton does, altering the results.

D. Results

Data were collected for Xenon and Krypton, but not Argon. Due to limitations of the experimental setup, the minimum temperature attainable after a lengthy cooldown of three to four hours was about 64 Kelvin. At this temperature, Argon does not experience any appreciable adsorption.

1. Xenon

The collected QCM data for Xenon follow. Error bars are set at +/- 0.8%. The individual plots for each temperature can be found in Appendix A. The first plot, in Figure 27 shows each temperature's contribution to the collective total. The second plot in Figure 28 shows all the data points with appropriate error bars and a trendline.

As evidenced by the data, the heat of adsorption decreases with coverage at low coverage, and then levels off, as predicted by the model. The data scatter at low coverage is mostly due to the 75 K set of points, which run 100-200 cal/mole higher than the others. This may be due to these data being taken at the end of a long bout of testing, during which time, heavy molecules (water vapor, carbon dioxide) that may leak into the tank at very low rates, could build enough of a condensed layer to provide a sloppy crystal surface, raising the low-coverage heat of adsorption. The heat of adsorption continues to decline after the monolayer level, but not at the steep pitch predicted for an ideal situation. If you exclude the 75 K data, the decline ends at 0.4 monolayer coverage. This agrees with a lot of heat vs. coverage plots found in the literature,[9,10,11] and is probably due to the second monolayer beginning in some clumps before the first monolayer is completed. This prevents a total flattening at mid-high (0.4-0.8) monolayer coverage, and arrests the expected decline at the 1-monolayer mark.

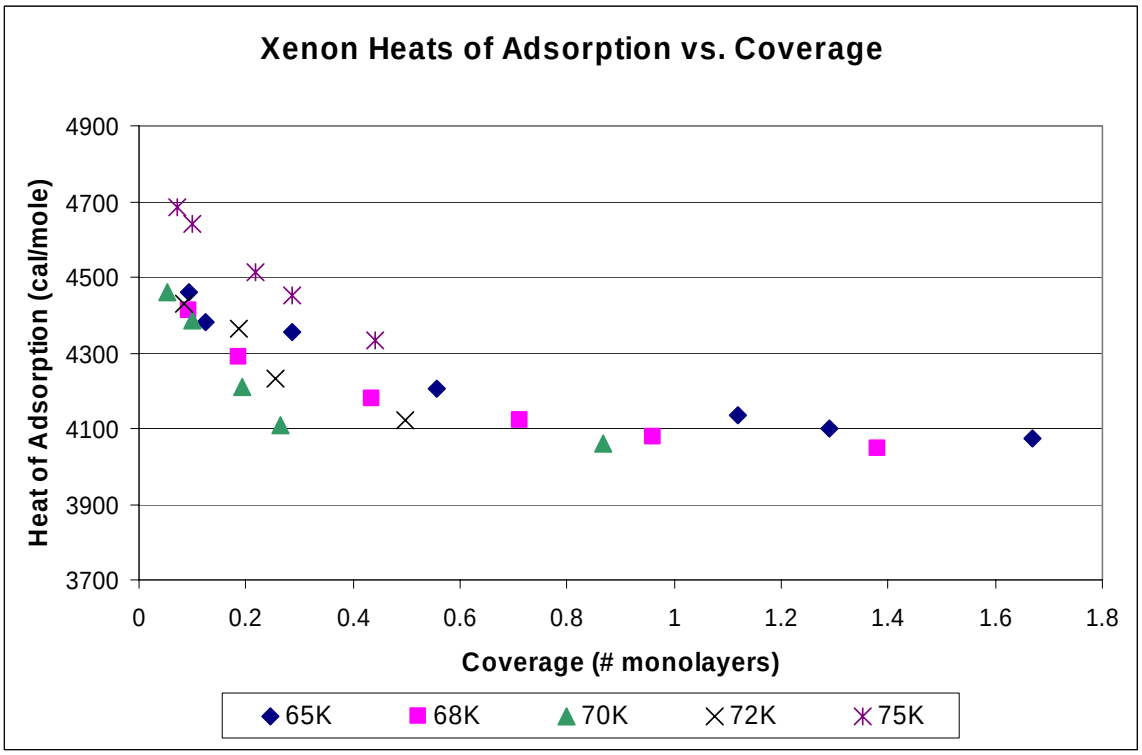

Figure 27. Xenon heat of adsorption vs. coverage, by temperature

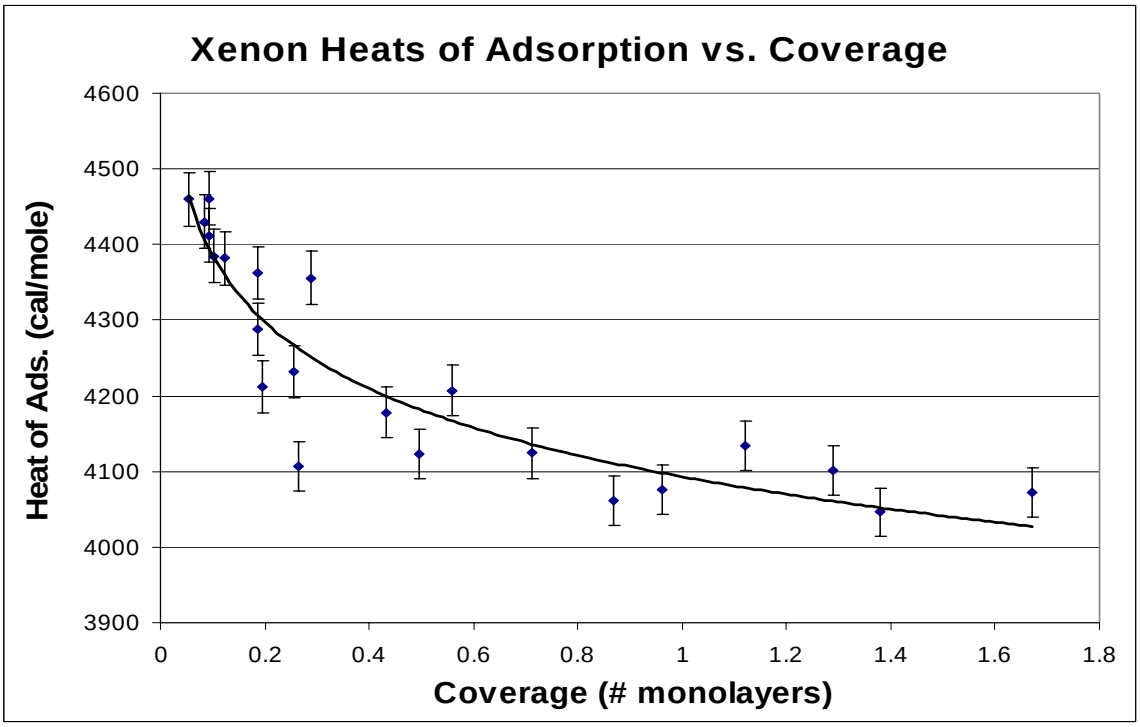

Figure 28. Xenon heat of adsorption data with trendline

After the low coverage decline is taken into account, the points seem to cluster around 4100 cal/mole for 0.6 to 1.2 monolayers. This is very close to the predicted value of 4050 cal/mole, which gives me pause, because I was expecting the experimental data to be 5-10% higher than predictions, due to the various non-idealities already mentioned: possible unevenness of the surface, possible pre-adsorbed heavy gas molecules such as water due to very minor leaks in the vacuum chamber, or impurities in the Xenon supply. The pressure is maintained in the low 10^{-8} to high 10^{-9} Torr range, but where the TPF will fly, the surrounding atmospheric pressure will be many orders of magnitude lower.

2. Krypton

The same plots used to display the Xenon data are now given for Krypton gas. Figure 29 shows all of the data points, denoted by the temperature at which they were gathered. Figure 30 shows all of the data points with +/- 1.0% error bars and a trendline. Individual plots can be found in Appendix A.

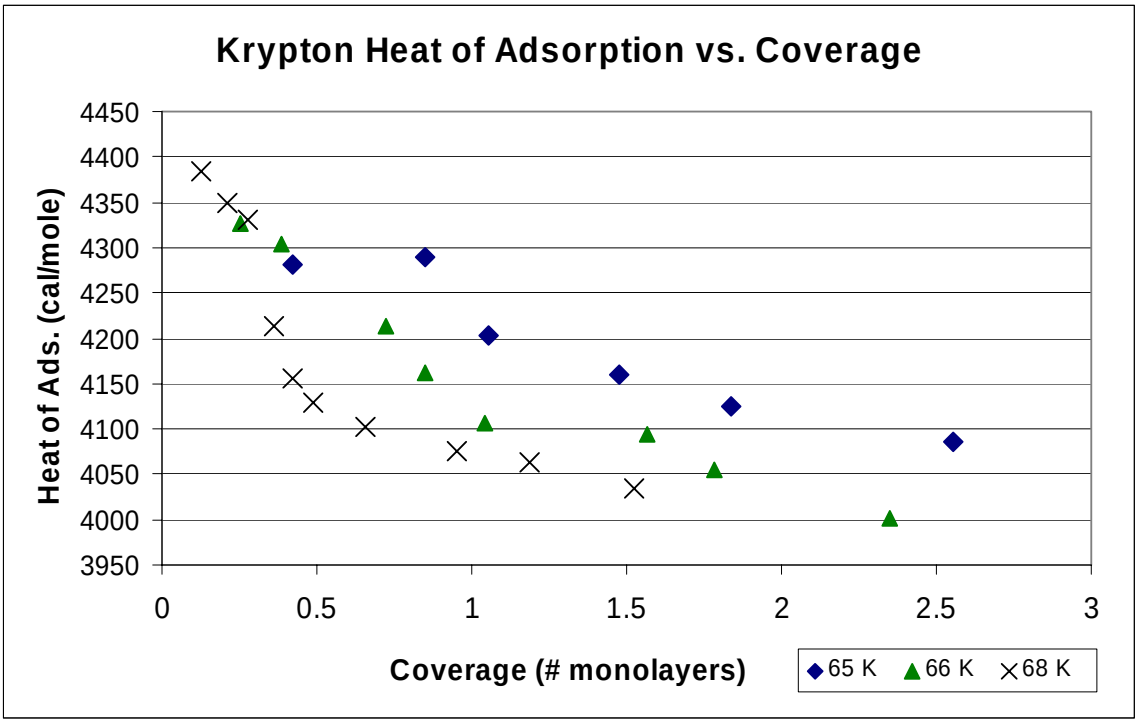

Figure 29. Krypton heat of adsorption vs. coverage, by temperature

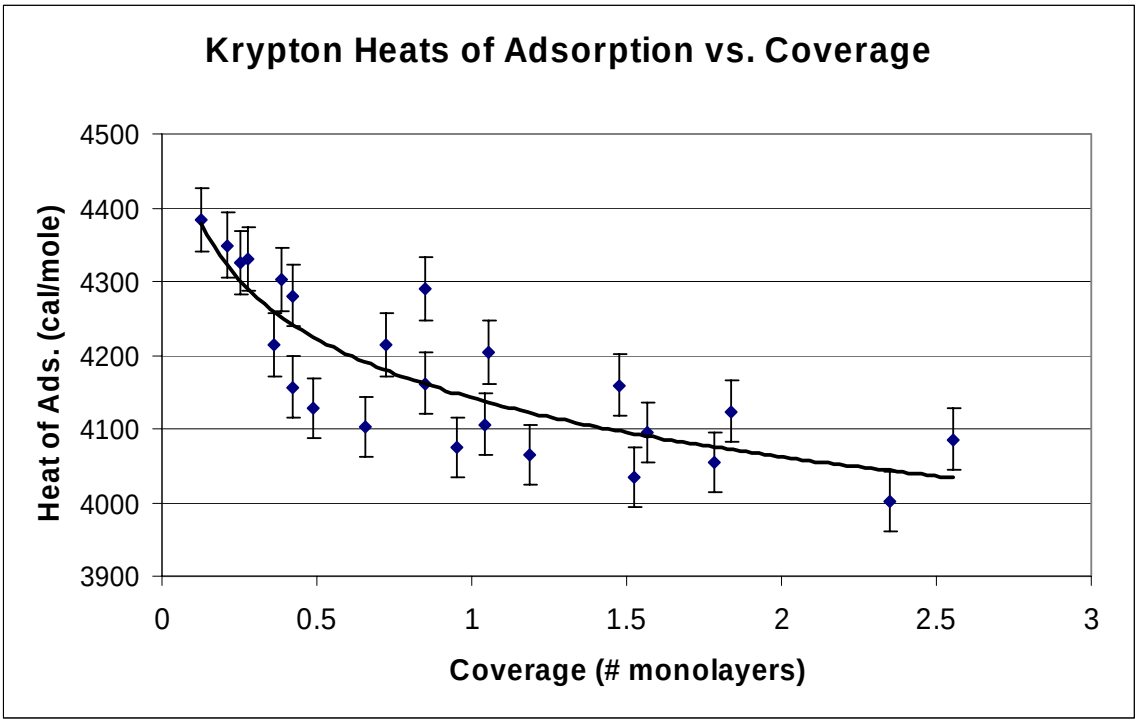

Figure 30. Krypton heat of adsorption data with trendline

The Krypton heat of adsorption data behaves very similarly to the Xenon data, although the values are higher than expected. It was expected that the Krypton line would be shifted down by 300-500 cal/mole from Xenon, but the experimental data here shows the trendlines to be nearly identical. This contradicts most of the literature read, which usually shows a considerable decrease when comparing the heat of adsorption of Xenon to that of Krypton. The reasons for this behavior may lie in the testing setup. While I think that the fact that Xenon is the primary impurity in Krypton specialty gas is a factor, it should be a minor one, since the impurity is in the tens of parts per million for 99.995% pure Krypton. Over a very long period of time, a considerable fraction of a monolayer of Xenon may develop at higher pressures, but the flux periods were kept under ten minutes. Another option is that by the time the QCM was cold enough to collect data (3-4 hours) that other species (H_2O, CO_2, Xe) had adsorbed to enough of an extent to obscure the gold surface. But on any surface, Krypton should have a lower heat of adsorption than Xenon. If this is the case, then there is no way to avoid that with this vacuum chamber. While its base pressure is in the low 10^{-8} Torr range, there are probably extremely tiny

leaks, which would let in outside air. With the humid Boston summer weather, this leads to water vapor. Pre-adsorbed material from before this project began should not be a concern, as the QCM is believed to be new. In retrospect, we should have tested krypton first, as there may have been some Xenon adsorbed on surfaces inside the tanks that kept outgassing during the Krypton tests. Of course, there is the very remote possibility that we received a Xenon bottle mislabeled as Krypton.

E. Interpretations

From the data shown, the model seems to fit for Xenon very closely. Krypton is reading higher than expected, as was explained in the last section. It was expected that hump at one monolayer would be considerably reduced, when taking into account the QCM surface being rougher than the TPF mirrors are expected to be, and also the competing phenomena of adsorbate-adsorbate interactions (which would cause the hump), and atoms sticking on top of already adsorbed gas atoms (which decrease the heat of adsorption). The low coverage behavior fits the model closely, showing a 10-12% increase at near-zero coverage, whereas 15% was modeled. Very little data beyond the monolayer level were taken for Xenon, as it is expected that even one full monolayer of deposition is undesirable. Some data were gathered for Krypton between one and three monolayers, and the heats at these coverage levels is definitely trending downwards. Predicting the post-monolayer behavior precisely requires a detailed knowledge of the condition of the surface before gas deposition has begun.

In this project, I feel that the experimental setup lets the model down to a certain extent, as it is not clean enough to allow the intricacies of the expected behavior to be uncovered without an ultra high vacuum system and perhaps a way to shield the QCM while the testing gas is not flowing. That being said, the model predicts the sub-monolayer behavior quite accurately, and at least for Xenon, seems to pinpoint the heat of adsorption very closely. The Krypton heat data came out quite a bit higher than expected, and thus could not confirm the model's behavior, although it fits well to other published data on different substrates.

VII. Recommendations

If a small multilayer deposition is acceptable, then Xenon may perform well enough. After a few monolayers have accumulated, the subsequent heat of adsorption should drop towards the heat of vaporization, which is 3015 cal/mole for Xenon. At 40 K this results in a residence time of just under 3000 seconds. If it is assumed that only the top layer of a multilayer deposition can desorb away, then a flux of under 2.17×10^{11} atoms/s/cm^2 will result in an equilibrium. Basically, for a deposition of 5.83×10^{14} atoms/cm^2 with a heat of adsorption of 3015 cal/mole, about 2.17×10^{11} atoms/cm^2 will desorb every second. For Krypton, the heat of vaporization is 2155 cal/mole, with a 40 Kelvin residence time of only 0.06 seconds. Here, a flux of over 10^{16} atoms/s/cm^2 would result in equilibrium, but the buildup would never reach that point, as that level of flux is infeasible for the thrusters considered for this mission, so far downstream. It is expected that the heat of adsorption will approach the heat of vaporization by five monolayers, and quite certainly ten monolayers, when starting with a clean, smooth surface.

However, if the maximum deposition must be kept below one monolayer, then the recommendations are more stringent. Xenon's high heat of adsorption results in a prohibitively high residence time, to the point where ongoing desorption is irrelevant for all but the smallest flux values. Even so, if the expected flux is expected to be of this very low order, less than 10^7 atoms/s/cm^2, then all that is required to keep the adsorption under a desirable level are annual bakeouts. Just raising the temperature to 60 Kelvin will bring the residence time of Xenon (experimental heat = 4100 cal/mole) down under two minutes. This results in over 99% of the deposition gone within ten minutes.

Judging by the experimental data, the same arguments apply for Krypton, but I'm skeptical, considering that the predictions for Xenon are on the same scale as those in the literature for other substrates, around 4000–4800 cal/mole. In addition the predicted heat for Krypton, 3236 cal/mole, is on the same order as the heats found for Krypton on varied substrates such as alumina, platinum, and graphitized carbon black, around 3300-3800 cal/mole.[10,16,17] I would venture that the realistic heat of adsorption for Krypton on a

clean and smooth gold surface would be 10% lower than the data here. Furthermore, due to the sloppiness of the QCM surface, I'd expect the realistic Xenon heat of adsorption to be 5% lower than the experimental data. A plot showing the expected deposition with continuous flux for Xenon and Krypton is given in Figure 31, both according to the experimental data, 5% lower for Xenon, and 5% and 10% lower for Krypton. This data are given in tabular form in Table 11. For the plots based on the experimental data, the coverages stop after three monolayers, because none of the data exceeded that level. The plots based on the model stop right around 1.1 – 1.2 monolayers, because of the modeled drop after the monolayer level. This basically halts deposition except at high levels of flux (> 10^9 atoms/s/cm^2). As explained, the experimental, and hence, the 95% plots for Xenon and Krypton nearly overlap.

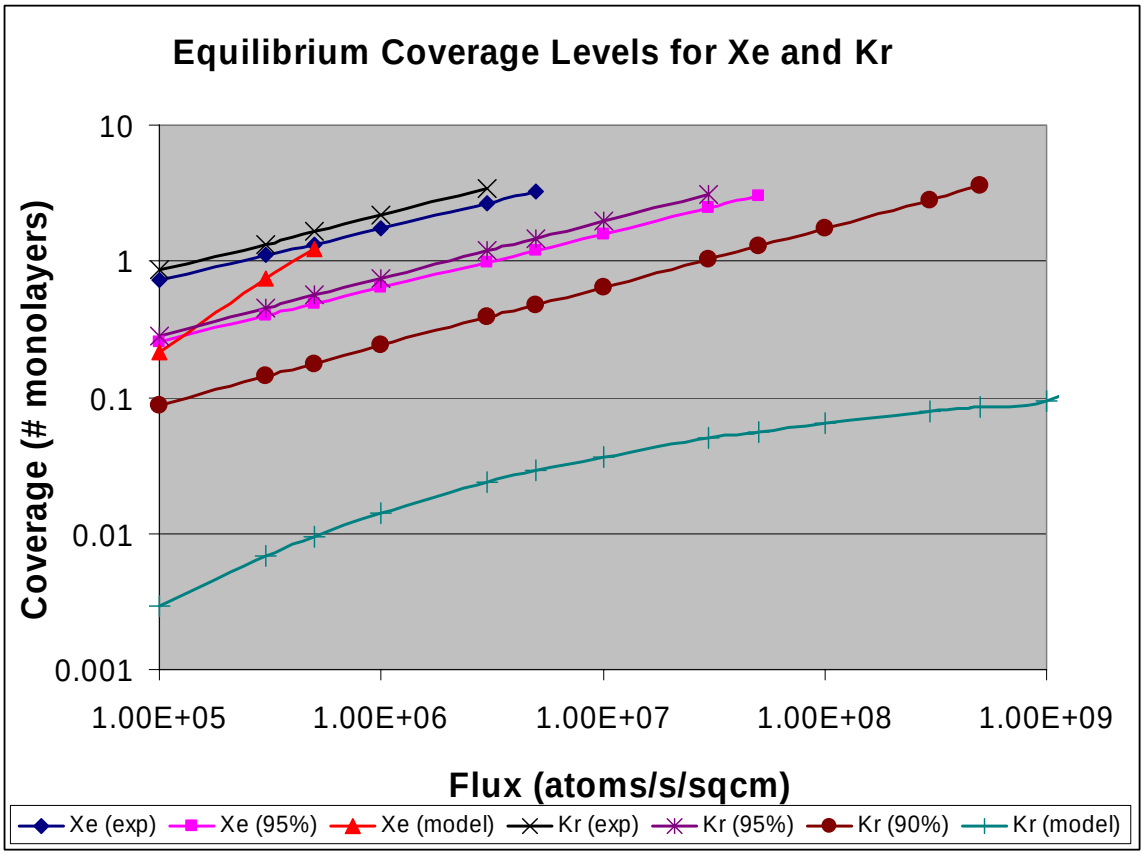

Figure 31. Expected equilibrium coverages for real and modeled data.

Flux	Xe (exp)	Xe (95%)	Xe (model)	Kr (exp)	Kr (95%)	Kr (90%)	Kr (model)	Ar (model)
1.0E+05	0.72	0.26	0.22	0.86	0.29	0.088	0.0029	
3.0E+05	1.11	0.40	0.75	1.34	0.45	0.14	0.0068	
5.0E+05	1.34	0.49	1.24	1.65	0.56	0.18	0.0095	
1.0E+06	1.75	0.64		2.19	0.75	0.24	0.014	
3.0E+06	2.66	0.99		3.42	1.19	0.39	0.024	
5.0E+06	3.24	1.21			1.47	0.48	0.029	
1.0E+07		1.59			1.97	0.65	0.036	
3.0E+07		2.46			3.12	1.04	0.050	0.0013
5.0E+07		3.01				1.30	0.056	0.0021
1.0E+08						1.76	0.065	0.0038
3.0E+08						2.83	0.079	0.0088
5.0E+08						3.56	0.086	0.012
1.0E+09							0.095	0.018
3.0E+09							0.22	0.030
5.0E+09							0.37	0.036
1.0E+10							0.75	0.045
3.0E+10							1.40	0.060
5.0E+10								0.068
1.0E+11								0.078

Table 11. Projected equilibrium coverages in tabular form for different coverages, values given in # of monolayers.

Using the 95% values, Xenon and Krypton remain under one monolayer of coverage up to a flux of 3.0×10^6 atoms/s/cm^2, while the 90% value for Krypton is at a monolayer at a flux of 3.0×10^7 atoms/s/cm^2, assuming that this flux is being received constantly. But even at the heat of vaporization of Xenon, which is 3015 cal/mole, the residence time is nearly an hour. Such is the drawback of using a heavy gas with a high boiling point.

Since the inherent atomic properties of the noble gases can not be altered, the flux must be reduced as must as possible to allow the use of Xenon or Krypton gas. There are three main recommendations to be made on the design end to help this cause. First, avoid firing the thrusters in the direction of the neighboring craft's mirrors as much as possible. The second recommendation is to shield the mirrors from the flux as much as possible,

including making the cylindrical shroud taller, lowering the probability that an atom will deflect at just the right angle to strike the mirror, particularly in such a collisionless environment. On that same idea, cooling surfaces immediately surrounding the mirrors to the same temperature or lower will also help remove stray atoms from the picture. With cooled walls, an atom must now go directly to the mirrors, without deflecting off of a wall. The last design recommendation is to incorporate regular warm-ups or bakeouts, whether it is monthly or yearly, provided the incoming flux is low ($\phi<10^8$ atoms/s/cm^2). The bakeouts would not need to be too warm, 65-70 Kelvin for thirty minutes is enough to release nearly all of the trapped gas.

My ultimate recommendation is to use the lightest propellant gas possible at as low a flux as possible. If Xenon must be used, it may be necessary to schedule periodic warm-ups to remove adsorbed propellant if the flux can not be reduced to low enough levels. If it turns out that the coverage must be kept under a monolayer, the flux must be very low for Xenon or Krypton to be feasible. If the coverage can be on the order of 10-20 monolayers, than either propellant can be used, because the heat of adsorption should decrease towards the heat of vaporization by that point, and then it's a matter of keeping the flux below the saturation vapor pressure of the propellant.

VIII. Conclusion

This project set out to determine whether or not propellant condensation upon gold-plated mirrors chilled to 40 K would be an issue for the Terrestrial Planet Finder team, and it is. After a lengthy period of literature researching and library browsing, the fundamentals behind adsorption and condensation were understood and applied to create a basic model that predicts the deposition rates and levels for various gases at varying fluxes impinging upon different surfaces depending on the surface temperature. The model predicted that Xenon propellant would condense heavily under all but the lowest flux rates, while Krypton could stand slightly higher rates of indirect flux. Argon, being such a light noble gas compared to the other two, would not adsorb to any worrisome degree unless applied at high levels of line-of-sight flux.

The model had to be checked against experimental data. A quartz crystal microbalance was used to measure mass that collects on its gold-plated surface. The QCM was mounted inside of a small vacuum chamber and a cryocircuit was placed around the QCM to cool it down to cryogenic temperatures. Liquid helium was used as the cryogenic fluid. There were substantial delays dealing with retrofitting the QCM for low temperature usage, as well as other delays diagnosing and mending small leaks in the vacuum chamber and also increasing the thermal contact between the QCM and the cryocircuit.

When data could finally be taken, the Xenon experimental data fit the model to a very precise degree within the first monolayer. Krypton was expected to have a lower heat of adsorption than Xenon, yet the data matched Xenon nearly exactly. Why that is the case is a mystery. Possible causes include a sloppy surface, impurities in the gas bottle, pre-adsorbed atom layers on the surface. Real-world usage of Krypton on a clean crystal surface should result in a decreased heat of adsorption of 10% or more from that of

Xenon, in accordance with nearly all previously published data that investigates both gases.

While the model or the setup seems to fall short on Krypton, the expected heat of adsorption vs. coverage trends are followed in both the model and experimental data. As Xenon is the propellant of most interest to the JPL TPF team, the fact that the model predicts the sub-monolayer heat of adsorption within a few percent gives validity to its construction. The end result of this research is a recommendation that JPL consider using lighter propellants if possible, and if heavier gases like Xenon and Krypton must be employed, that the flux impacting the mirrors be made as minimal as possible through the use of shielding, cooling the surrounding surfaces, pointing the thrusters away from the vicinity of the mirrors, and periodic warm-ups to 65 K or 70 K.

Appendix A – Data Plots

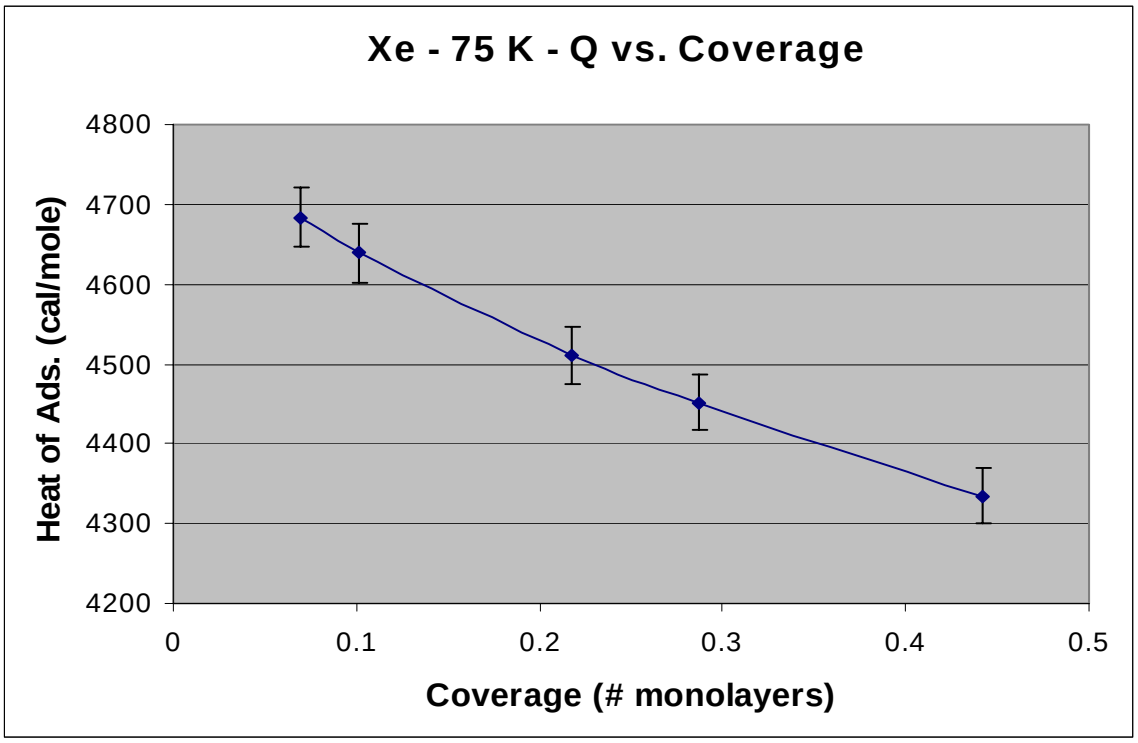

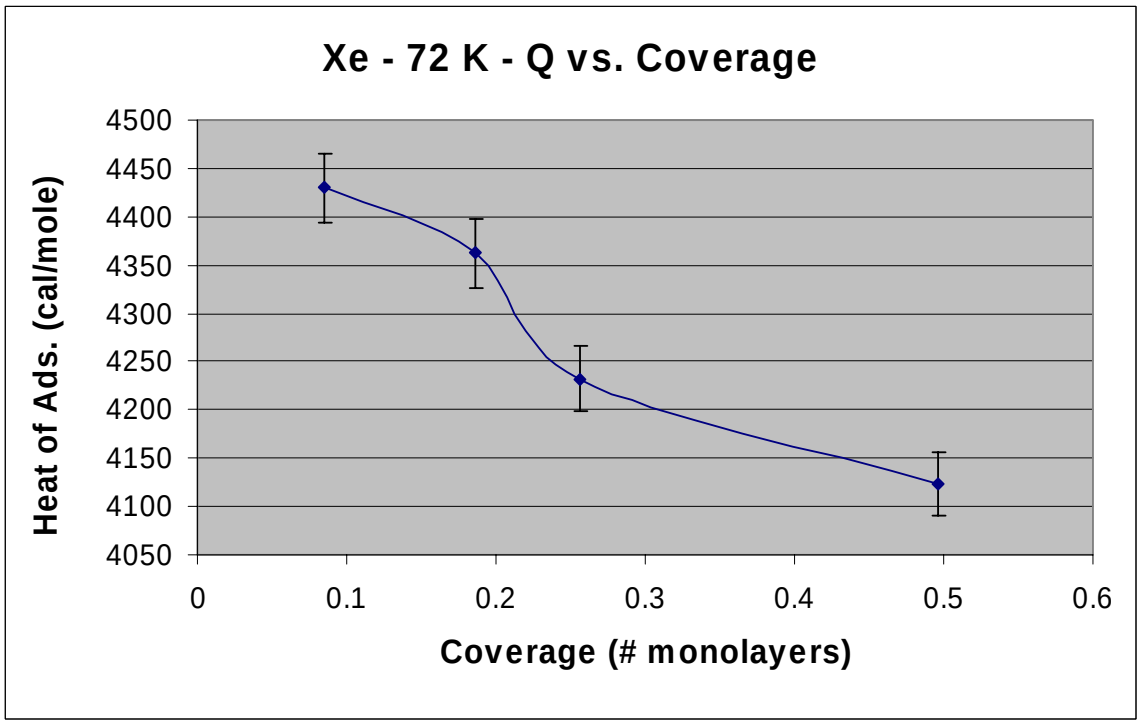

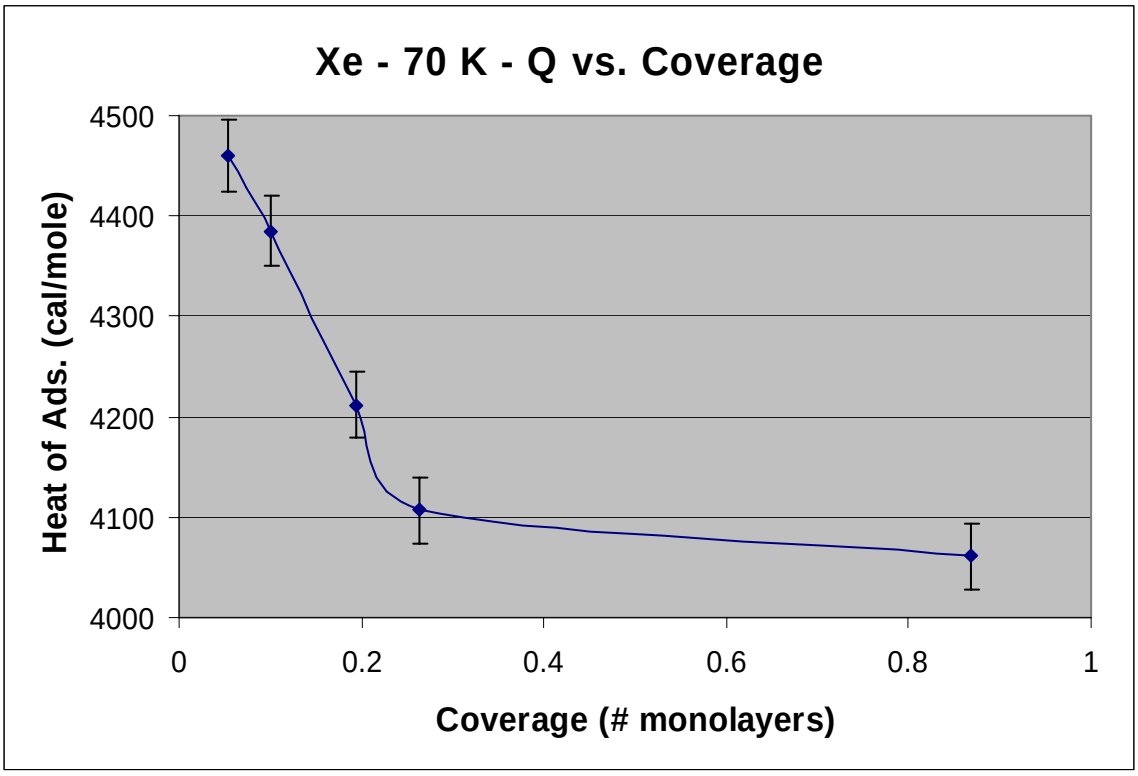
Xe - 70 K - Q vs. Coverage
Heat of Ads. (cal/mole)
4500
4400
4300
4200
4100
4000
0
0.2
0.4
0.6
0.8
1
Coverage (# monolayers)

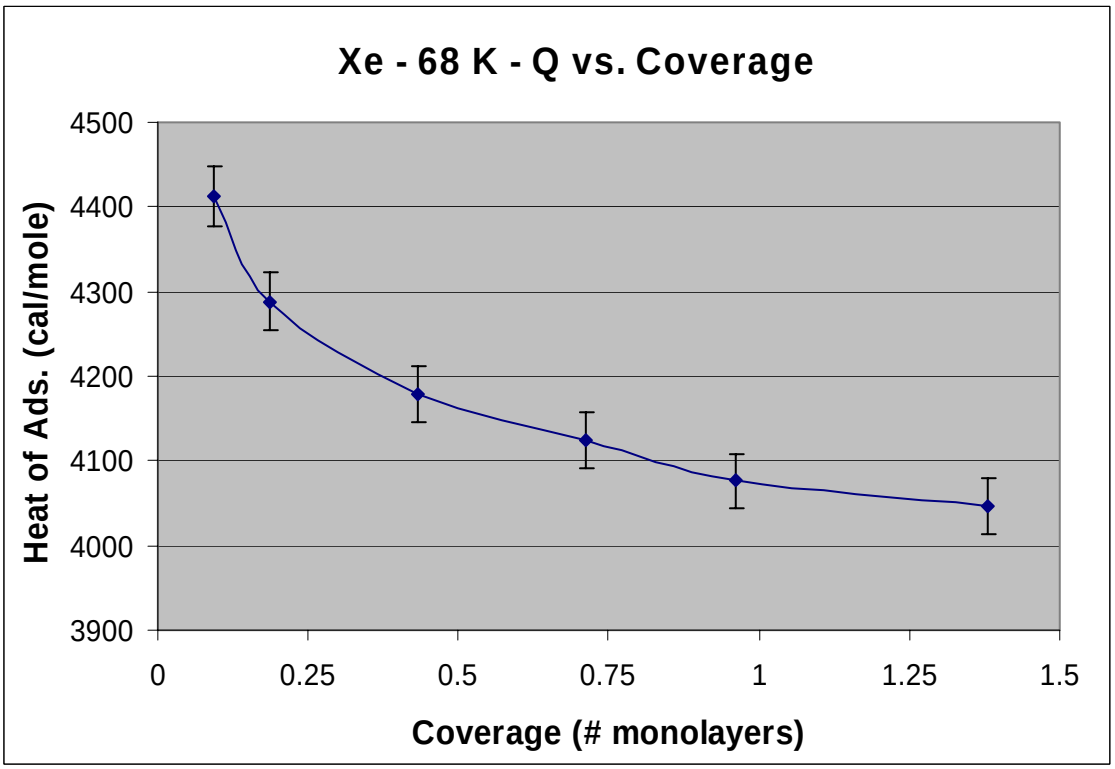
Xe - 68 K - Q vs. Coverage
Heat of Ads. (cal/mole)
4500
4400
4300
4200
4100
4000
3900
0
0.25
0.5
0.75
1
1.25
1.5
Coverage (# monolayers)

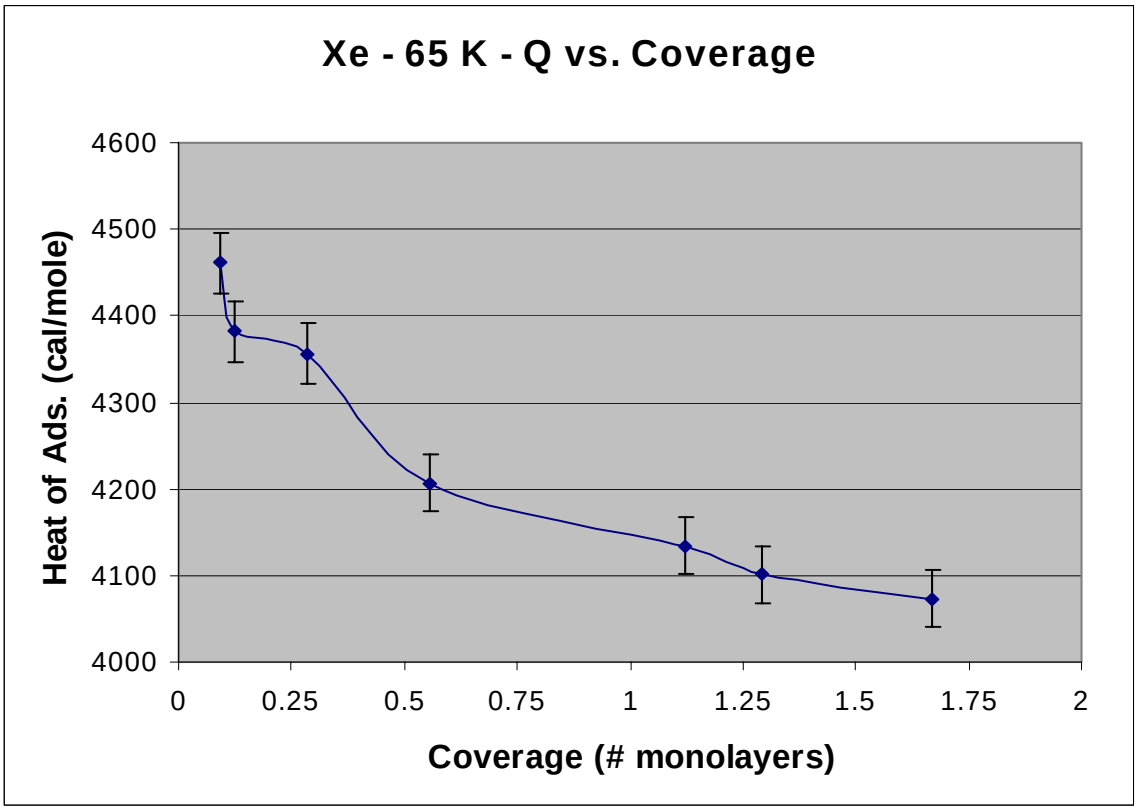

Figure A1-A5. Xenon plots at each temperature

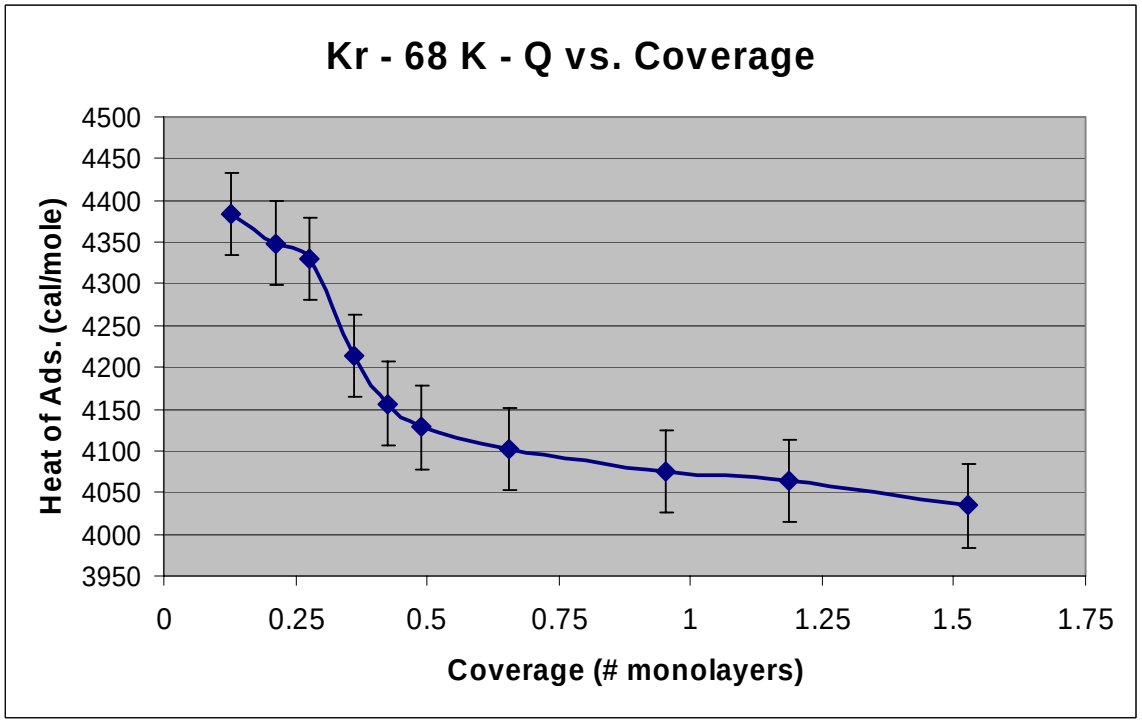

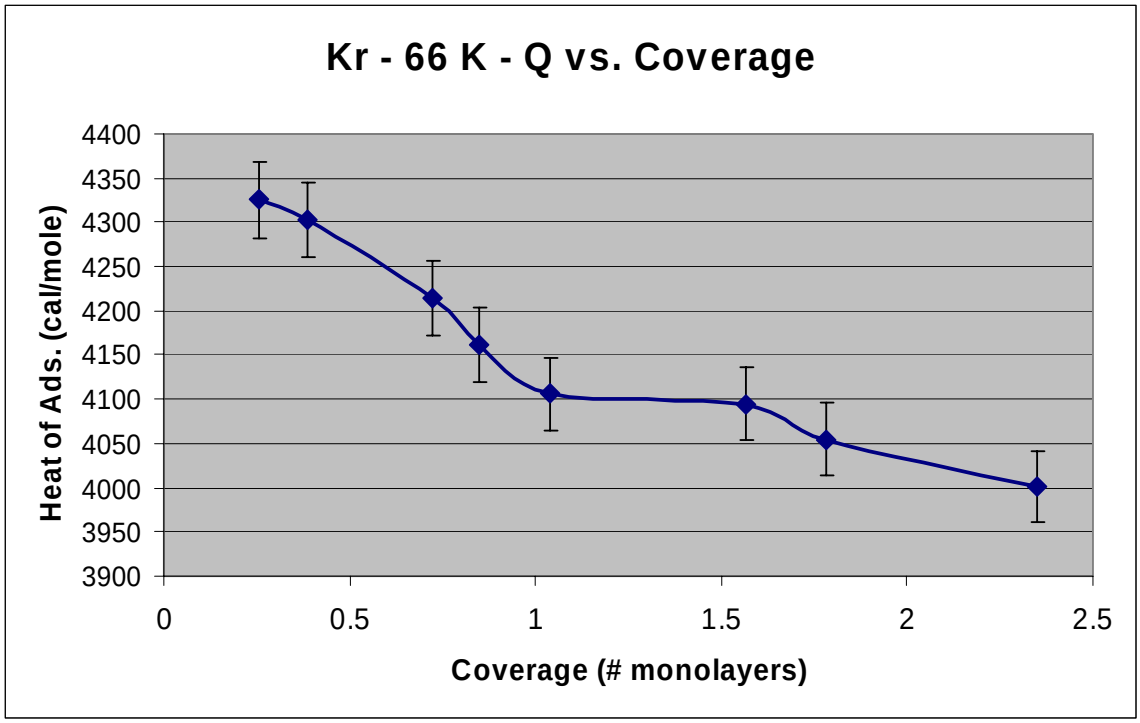

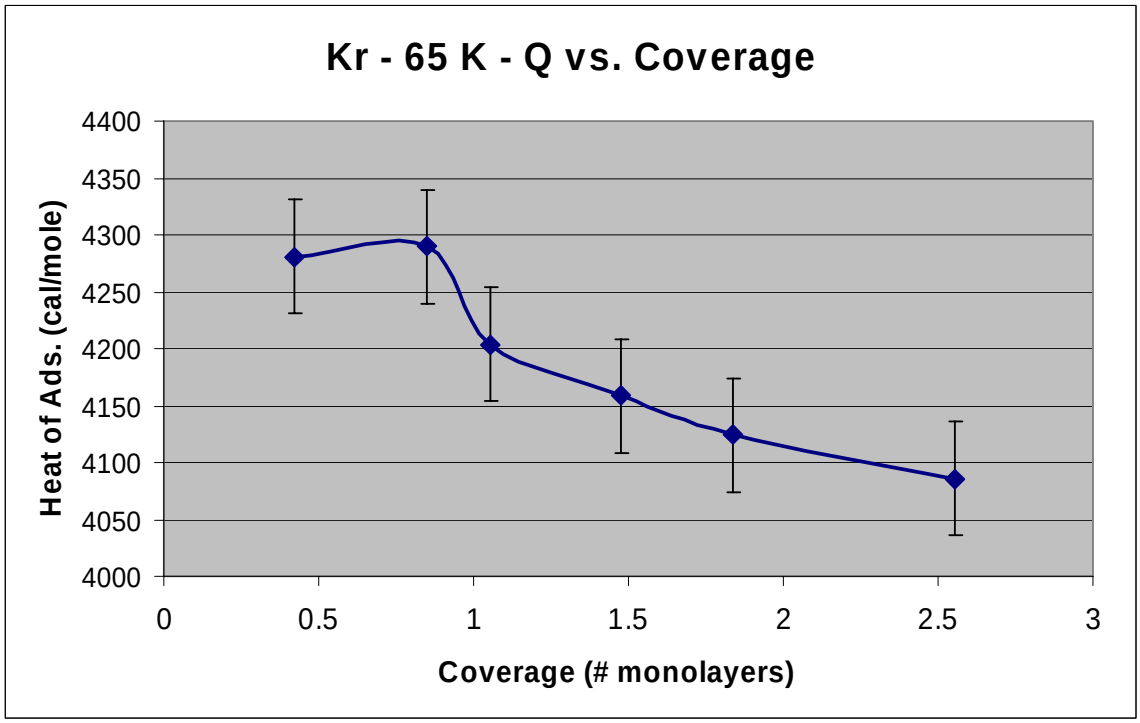

Figure A6-A8. Krypton plots at each temperature

Appendix B – Instructions

A. Using Liquid Helium

1. Call 253-2215 to order liquid helium from the MIT Cryogenics Lab in building 41. They sell liquid helium for $4.50/liter, and the available quantities are 30, 60, and 100-liter dewars. A 30-liter dewar should last one long day of testing, about 8+ hours of usage.

2. Hook up the appropriate fittings to one end of the double feedthrough to fit the adapter that should be on the liquid helium transfer tube. The tube has a threaded 3/8" ending. The adapter has a threaded hole that screws onto the transfer tube. On the other end of the adapter is a ¼" female Swagelok nut.

3. Attach the insulated helium vent line to the other side of the double feedthrough and stick the free end into the fume hood.

4. The helium dewar will have 6 lines coming out of the top. Line A is the port that goes straight down into the dewar, that is threaded on the outside, with a valve handle. Lines B-F come out at 90 degrees from Line A. Line B is a pressure gauge that reads to about 15-30 psi overpressure. Line C is has a valve handle and an open female end, about ¾" in diameter. Line D is a small relief valve with a valve handle. This relief valve opens at about 2-3 psi, so keep it shut unless you need to relieve pressure. Lines E and F are high-pressure relief valves that usually open at around 8-10 psi. A diagram is given in the Figure B1.

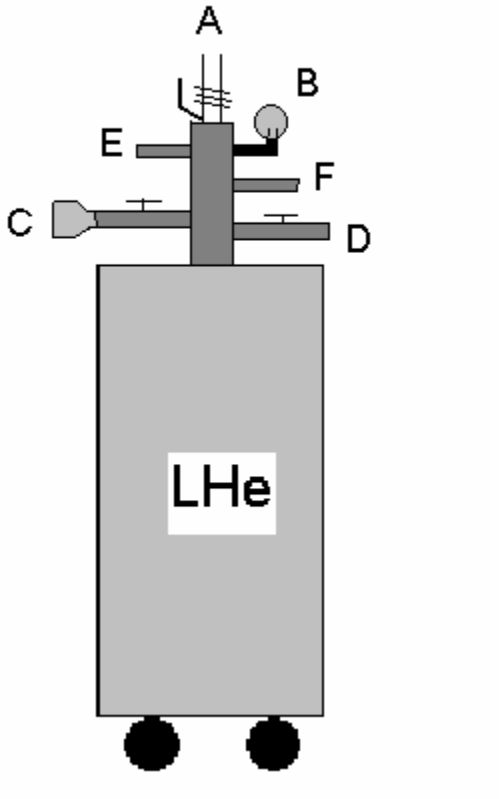

Figure B1. Liquid helium dewar ports

5. Attach the transfer tube's fitted end to the double feedthrough, and make sure that the valve for Line D is open. Now slide the brass transfer tube adapter up the shaft of the transfer tube. Stick the tube in Line A. It will only go in about 2" because the valve is shut. Slide the transfer tube adapter down and tighten the bottom nut around the Line A port.

6. Put on the yellow cryogenic safety gloves and face shield. Now open the valve on Line A and slide the transfer tube down slowly. When it contacts the bottom, pull it back up an inch or two. As it nears the bottom, a hissing sound will be heard, and the relief valves will probably open. Now tighten the upper nut of the transfer tube adapter and the hissing from the Line A port will stop. Also shut the Line D relief valve. Helium will now be flowing.

7. Watch the pressure gauge, and slowly open the Line D valve and let off pressure until it drops to about 2-3 psi. An appropriate pressure for flowing liquid helium is 1.5-2.5 psi.

8. Wheel over the large helium gas tank that resides in the lab. Screw the fitting cluster into the Line C port that fits it and has a Teflon barb on the other end. Stick the flexible helium gas tube onto the barb, and pressurize the regulator to >10psi. When the pressure in the helium dewar drops below 1.5 psi, open the Line D valve slowly until the pressure rises to the desired level. When trying to get down to 65K, it may be necessary to raise the dewar pressure to 3 psi.

9. The QCM should be running the entire time, logging the cooldown. Kill the heaters. The temperature should reach 200 K after a half hour or so, and 130 K after an hour. After two hours, the temperature should be under 80 K.

10. When finished testing, get one person to assist. Detach the transfer tube from the vacuum chamber feedthrough. Have the helper hold that end upright. Don the gloves and mask. Loosen the top nut of the transfer tube adapter on the dewar. Slowly pull the tube out of the dewar. When the tube is just about out, close the Line A valve. Now loosen the bottom nut and slide the adapter up the tube and put the transfer tube somewhere safe. Make sure all of the dewar valves are closed. Helium will evaporate overnight, but if the pressure gets too high, the high-pressure relief valves will open.

11. There will be condensation over all the pipes and insulation, so cover up any electronics that may get dripped on as the pipes warm and the condensation melts.

B. Using Liquid Nitrogen

1. To order liquid nitrogen, call the MIT Cryogenics Lab at 253-2215. Liquid nitrogen is cheap at $0.19/liter, but the smallest dewar available is 160 liters, so order that.

2. If using liquid nitrogen to cool down the QCM for higher temperature condensation testing above 110 K, then hook up the vent line to one end of the double feedthrough.

3. The liquid nitrogen dewar has 4 ports. All coming out parallel to the floor. Line A is just a relief valve that can not be turned on or off. Line B is a pressure gauge. Line C has a valve and a male threaded end and says “VENT” above it. This is to draw off nitrogen gas. Line D has a valve and a male threaded end as well. This is for drawing out liquid.

4. Using liquid nitrogen is far simpler than helium. Don the gloves and mask. Hook up a pipe from the liquid port on Line D to the other end of the double feedthrough, then just open the valve to a desired flow level.

5. If using to cool down the double feedthrough, but cooling the QCM with helium, then attach a long 1/8” copper tube to the liquid port, coil tightly around the feedthrough, and vent the nitrogen into the fume hood.

6. When finished using the nitrogen, just shut off the valve on line D.

7. There will be condensation over all the pipes and insulation, so cover up any electronics that may get dripped on as the pipes warm and the condensation melts.

C. Flowing the Test Gas

1. Hook up a thin capillary line to a 1/16" Swagelok adapter, and adapt that up to a ¼" female Swagelok end to hook to the gas feedthrough line. Plug the other end of that capillary into the micrometering valve

2. Adapt down from a gas regulator to a capillary line and hook the other end of the capillary into the supply end of the micrometering valve. Connect a gas bottle to the regulator. The thinner the capillary, the smaller flows are permitted.

3. On the vacuum chamber cold-cathode pressure gauge, set the appropriate gas correction factor for the test gas. Xenon – 2.9, Krypton - 2.1, Argon – 1.3, air - 1.0.

4. Open the bottle valve, and set the regulator pressure as low as possible, 3-5 psi is a low enough.

5. When ready to test, SLOWLY open the micrometering valve until the pressure levels off at a desired level. It is nearly impossible to hit a specific pressure, so aim for a range. Instead of shooting for 3.5×10^{-6} Torr, aim for $3.0\text{-}4.0 \times 10^{-6}$ Torr.

6. When finished, close the micrometering valve, the regulator valve, and the bottle valve.

D. Operating the QCM Software

1. Turn on the computer, once loaded to the desktop, turn on the switch on the front of the M2000 data box.

2. Start the "QCM Model 2000" program, all the settings on the first screen should be set right for this QCM. The modified QCM is serial number 2996. Click OK to go to the next screen.

3. Hit "START". It will prompt a form where you can enter the tester's name, purpose, and change the filename. After it is to your liking, hit OK, and data collection will begin.

4. Set the graph and log time to 15 seconds or greater during cooldowns, and periods where data is not being taken. Open up the log or graph if desired.

5. When data is being taken, set the log time to 1 second, and data will be taken at the rate of 1 Hz.

6. When finished, hit "STOP". To start a new data log, hit "START" and repeat from step 3. If you are finished taking data, close down the program and shut off the M2000 unit.

Citations

[1] "Terrestrial Planet Finder", TPF Science Working Group, edited by C.A. Beichman, N.J. Woolf, and C.A. Lindensmith, NASA Jet Propulsion Laboratory, JPL publ. 99-003, California Institute of Technology, Pasadena, CA, May 1999.

[2] Chen. P.T., Thomson, S., Woronowicz, M.S., "Applying Contamination Modeling to Spacecraft Conventional Propulsion System Designs and Operations", *AIAA Journal of Spacecraft and Rockets*, vol. **38**, no. 3., May-June 2001, pp. 388.

[3] Scialdone, J.J., "Self Contamination and Environment of an Orbiting Satellite", Journal of Vacuum Science, vol 9, no. 2, July 1971.

[4] Chang, C.W., "Application of General Sticking Coefficient Models to Spacecraft Contamination Analysis", SPIE vol. 3784, #0277-786X/99, 1999.

[5] Walker, Gallimore, Boyd, "Vacuum Chamber Pressure Maps of a Hall Thruster Cold Expansion Flow", *AIAA Journal of Propulsion and Power*, Vol 20. No. 6. 2004.

[6] Goodman, F.O., "On the Theory of Accommodation Coefficients V. Classical Theory of Thermal Accommodation Trapping," *Rarefied Gas Dynamics, Supplement 3*, Vol. 2, Academic Press, Inc., 1966.

[7] Gregg, S.J., Sing, K.S.W., *Adsorption, Surface Area, and Porosity*, Academic Press, London, 1967.

[8] Yang, R.T., *Adsorbents: Fundamentals and Applications*, John Wiley and Sons Publications, Hoboken, NJ, 2003, pp. 8-25.

[9] Pace, E.L., Siebert, A.R., "Heats of Adsorption and Adsorption Isotherms for Low Boiling Gases Adsorbed on Graphon", *Journal of Physical Chemistry*, v. **64**-8, 1960, pp. 961-963.

[10] Chon, H., et al, "Interaction of Helium, Neon, Argon, and Krypton with a Clean Platinum Surface", Journal of Chemical Physics, v. **36**-5, 1962, pp. 1378-1382.

[11] Wong, A., Zhu, X.D., "An Optical Differential Reflectance Study of Adsorption and Desorption of Xenon and Deuterium on Ni(111)", *Applied Physics A*, vol. **63**, 1996, pp. 1-8.

[12] Mueller, J., et al, "JPL Micro-Thrust Propulsion Activities", AIAA Nano-Tech 2002, AIAA paper 2002-5714

[13] Santi, M., et al, "Further Development and Preliminary Results of the AQUILA Hall Thruster Plume Model", 39th AIAA Joint Propulsion Conference, AIAA paper 2003-4873, July 2003.

[14] Alexeenko, A.A, et al, "Measurements and Simulation of Orifice Flow for Micropropulsion Testing", *AIAA Journal of Propulsion and Power*, vol **19**, no. 4, July-August 2003. pp. 588.

[15] Ketsdever, A.D., "An Overview of Ground Based Spacecraft-Thruster Interaction Studies: Facility Design Issues", 38th AIAA Aerospace Sciences Meeting and Exhibit, AIAA paper 2000-0463, January 2000.

[16] Moulik, S.P., "A Correlative Treatment of the Heat of Adsorption with Coverage on the Monolayer Side", *The Journal of Physical Chemistry*, vol **70**, no. 10, October 1966. pp. 3346

[17] Hobson, J.P., "Pumping at Solid Surfaces", *British Journal of Applied Physics*, vol **14**, 1963, pp. 544.